ELSEVIER

Chemical Geology 195 (2003) 229–273

CHEMICAL GEOLOGY
INCLUDING
ISOTOPE GEOSCIENCE

www.elsevier.com/locate/chemgeo

A tale of shales: the relative roles of production, decomposition, and dilution in the accumulation of organic-rich strata, Middle–Upper Devonian, Appalachian basin

Bradley B. Sageman[a,*], Adam E. Murphy[b], Josef P. Werne[c], Charles A. Ver Straeten[d], David J. Hollander[e], Timothy W. Lyons[f]

[a] *Department of Geological Sciences, Northwestern University, Evanston, IL 60208, USA*
[b] *Millbrook School, School Road, Millbrook, NY 12545, USA*
[c] *Department of Marine Biogeochemistry and Toxicology, Netherlands Institute for Sea Research (NIOZ), P.O. Box 59, 1790 AB Den Burg, Texel, The Netherlands*
[d] *Center for Stratigraphy and Paleontology, New York State Museum, The State Education Department, Albany, NY 12230, USA*
[e] *College of Marine Science, University of South Florida, St. Petersburg, FL 33701, USA*
[f] *Department of Geological Sciences, University of Missouri, Columbia, MS 65211, USA*

Received 31 July 2001; received in revised form 10 June 2002

Abstract

A new consensus on the processes responsible for organic carbon burial in ancient epeiric seas has emerged. More firmly grounded in the uniformitarian framework of modern oceanography and biogeochemistry, this consensus recognizes the interdependent roles of sedimentation, primary production, and microbial metabolism in favor of earlier end-member models (e.g., "production vs. preservation"). In this study, one of the classic stratigraphic sequences upon which the "preservation" end-member was based is re-interpreted in light of this new consensus. The study employs an extensive new sedimentological–biogeochemical database from cores drilled in western New York. The database spans over 500 m and 15 my of Devonian deposition in the Appalachian basin and provides a framework for comparative study of organic matter burial. The major conclusions are: (1) few organic-rich units were deposited under pervasive anoxic–sulfidic water columns; (2) establishment and breakdown of seasonal thermoclines, on annual or longer timescales, were the predominant mode of stratification; and (3) under such conditions, remineralization of bio-limiting nutrients may have played a key role in organic matter burial by creating a "eutrophication pump." This pump may have augmented an already rising nutrient inventory such that productivity levels exceeded the threshold required for development of suboxic to anoxic conditions in sediments, and episodically in bottom waters. A final conclusion asserts that the master variable for organic matter accumulation was relative sea-level change, which exerted influence on clastic dilution, preservation, and production processes. Sea-level rise events led to sediment starvation and organic carbon concentration in distal basin sediments, as well as to decreased effectiveness of seasonal mixing and thus longer build-up intervals for remineralized nutrients. Episodic mixing of nutrient-enriched bottom waters led to enhanced production. Ultimately, increased clastic sediment delivery and water column mixing during relative sea-level fall diluted surface sediment

* Corresponding author.
E-mail address: brad@earth.northwestern.edu (B.B. Sageman).

0009-2541/03/$ - see front matter
doi:10.1016/S0009-2541(02)00397-2

organic content such that respiratory demand could be met by increased oxygen supply, thus terminating deposition of strata enriched in organic carbon.

Keywords: Shales; Middle–Upper Devonian; Appalachian basin

1. Introduction

Ancient organic carbon-rich facies have long attracted geological interest (e.g., Pompeckj, 1901; Grabau, 1913; Schuchert, 1915). In the latter half of the 20th century, this interest was intensified through the efforts of the petroleum industry to understand the nature and origin of source rock facies. This resulted in application of the latest geological technologies to the study of fine-grained strata and oxygen-deficient basins (Demaison and Moore, 1980), and significantly advanced the field. Reports on organic carbon-rich deposits from practically every marine and lacustrine environment where they form and virtually every geologic age in which they occur, including the modern, can now be found in the literature. In these studies, some of the first biogeochemical techniques were developed and integrated with stratigraphic and sedimentologic observations. In recent decades, it has been increasingly recognized that organic matter (OM) burial in marine sediments represents an important variable in linked global biogeochemical cycles and is thus critical to understanding the history of oceans, the atmosphere, and climate change (e.g., Arthur et al., 1988; Berner, 1990; Berner and Canfield, 1989; Van Cappellen and Ingall, 1994). Integrated stratigraphic and biogeochemical databases have played a key role in this work. The first major objective of this paper is to document the development of one such new database from geochemical analysis of core samples representing fine-grained basinal deposits of the Devonian Appalachian basin, western New York State. This database is specifically designed to address the causes of extensive burial of organic matter in shallow epicontinental seas (≤ 300 m at maximum highstands) during the mid- to Late Devonian greenhouse and the consequences of this process for marine ecosystems and climate change.

The critical questions in all studies of geological processes focus on the controlling or limiting factors that govern the rate, direction, and magnitude of change. Over the past two decades, a general consensus has emerged about the controls on organic matter burial in which three factors are acknowledged as fundamental to the formation of almost all organic carbon-rich facies (e.g., Suess, 1980; Emerson, 1985; Emerson and Hedges, 1988; Arthur and Sageman, 1994; Canfield, 1994; Wignall, 1994; Tyson, 1995). They are primary photosynthetic production, bacterial decomposition, and bulk sedimentation rate, or dilution (Fig. 1). These controls can be correspondingly thought of as the rate at which carbon is fixed and exported from surface waters, the rate at which it is remineralized to CO_2 in the water column and sediments, and the rate at which organic carbon is buried relative to the flux of detrital dilutants (processes represented geochemically in Fig. 2).

Despite this consensus, significant differences remain among researchers concerning the relative importance of each of these processes. Although modern data suggest that OM concentration increases with increasing bulk sedimentation rate (Bralower and Thierstein, 1984; Henrichs and Reeburgh, 1987; Betts and Holland, 1991), at least up to a threshold of dilution (Ibach, 1982; Tyson, 1995), most ancient organic-rich deposits in epeiric settings appear to have accumulated under very low bulk sedimentation rates. If ancient depositional environments were permanently anoxic, this appears to outweigh modulation of concentration by sedimentation effects (Stein, 1986, 1990; Tyson, 1995, 2001), but many epicontinental basin deposits show evidence of at least intermittent, if not frequent events of oxygenation (Sageman et al., 1991; Oschmann, 1991; Wignall, 1994). It has also been suggested that high primary production dominates in controlling ancient organic matter burial (Pedersen and Calvert, 1990). However,

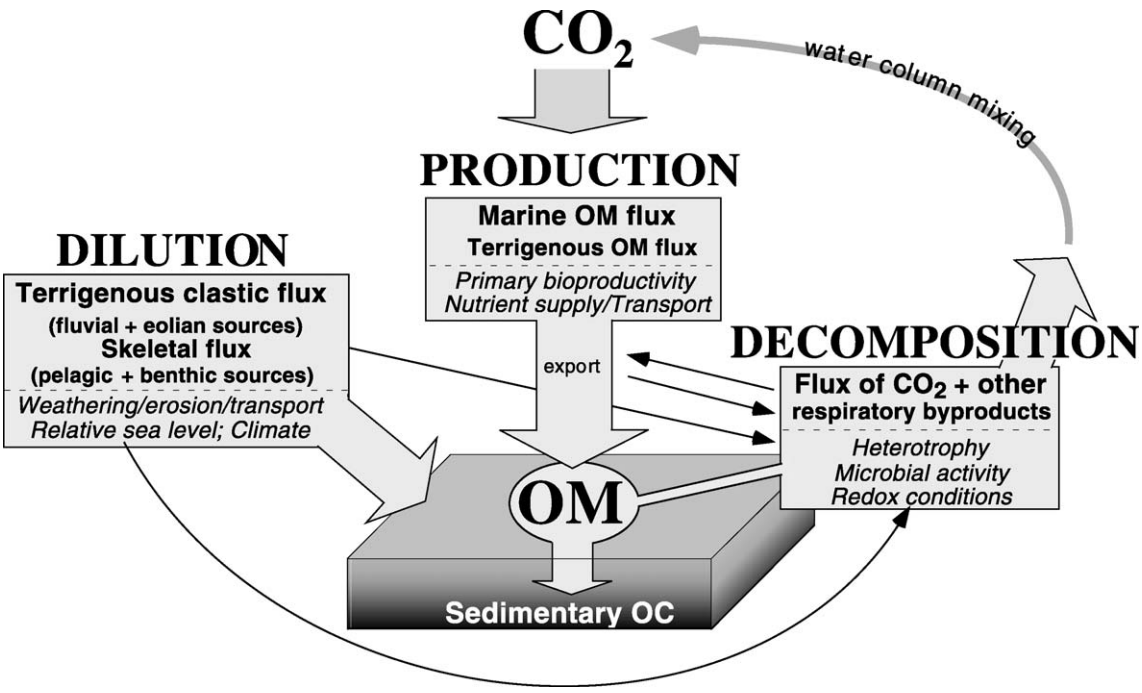

Fig. 1. The three fundamental processes that regulate burial of organic matter in marine sediments. The proximate controls on these processes are listed below the dashed line in each box. Note linkages between proximate controls (thin arrows), such as relative sea-level and export production, which both influence benthic redox conditions, which, in turn, may influence recycling of nutrients (see text for further discussion).

data from high sedimentation regimes, such as the modern continental margins on which the productivity hypothesis is based, may provide a biased view of OC accumulation processes in ancient epeiric seas (Tyson, 2001). Recently, the impact of changes in planktonic ecosystems on OM accumulation and autodilution processes (Tyson, 1995; Werne et al., 2000), changes in organic matter type and reactivity on preservational potential (Gong and Hollander, 1996), variations in water depth and its effect on OM delivery flux to the sea floor (e.g., Sarnthein et al., 1992; Tyson, 2001), and the contribution of bacterially sourced OM to bulk sedimentary OC (e.g., Kuypers et al., 2002) have received increasing attention. Clearly, there is a continuum of processes that vary among different depositional environments and geological periods. In each case, the relative importance of these different processes must be independently evaluated, if possible. The second major objective of this study is the development/refinement of a proxy methodology (see Fig. 2) to assess the relative roles of organic matter production, decomposition, and dilution in ancient OC-rich strata.

Integration of these two objectives in the context of a detailed stratigraphic and sedimentologic framework for a thick sequence of fine-grained strata in the Devonian Appalachian basin allows a comparative approach. This ‘‘tale of shales’’ encompasses the full range of changes experienced in the distal (basinal) facies tract. Based on this comparison, a new depositional model for Late Devonian black shales of the Appalachian basin is proposed. Description of this model is the third major objective of the paper. The model takes into account the sea-level history, paleogeography, and paleoclimate of the basin, as well as hypotheses about water depth, seasonal stratification, and the frequency and effectiveness of water column mixing. The central feature of this depositional model, and that which represents a departure from prior models for these Devonian black shales, is the role played by microbial communities (Fig. 2) in the breakdown of sedimentary OM and release of bio-

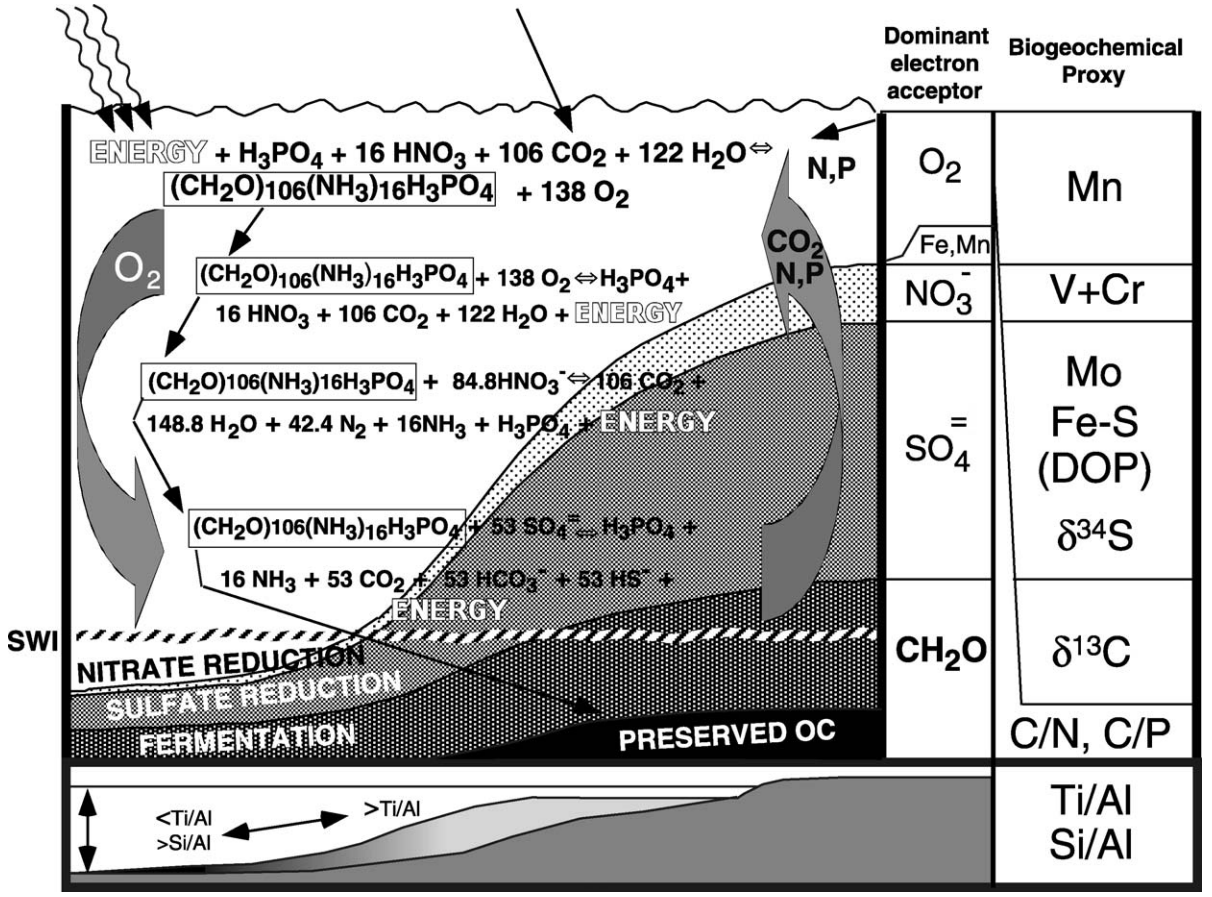

Fig. 2. Illustration of the photosynthetic fixation of carbon in marine organic matter, and its subsequent remineralization under dominant microbial regimes (aerobic, anaerobic-denitrifying, anaerobic sulfate-reducing, and anaerobic-fermentative) is shown in relation to biogeochemical proxies used in this study. Increased accumulation of the indicated proxies is interpreted to reflect the relative (temporal) dominance of different processes in time-averaged mudstone samples. Changes in the ratios of Ti and Si to Al are interpreted to reflect changes in detrital delivery (e.g., Bertrand et al., 1996). Accumulation of a series of redox-sensitive metals reflects the succession of microbial regimes under which OM is degraded (Berner, 1980): Mn accumulation typically indicates oscillating redox conditions (Calvert and Pedersen, 1996); similarly, oscillation through the zone of denitrification may result in relative increases in the value of V + Cr (Piper, 1994); pyrite Fe and Mo accumulate under sulphate reducing conditions, but are influenced also by changes in sedimentation rate (Raiswell et al., 1988; Canfield et al., 1996; Lyons, 1997; Raiswell and Canfield, 1998; Emerson and Huested, 1991; Crusius et al., 1996; Piper, 1994; Helz et al., 1996); significant depletion of $\delta^{34}S_{pyr}$ is generally indicative of prolonged euxinia (Lyons, 1997). If there are no major changes in OM source (Meyers, 1994), increases in C/N and C/P ratios of preserved OM may reflect decompositional losses of N and P due to microbial processes (Aller, 1994; Van Cappellen and Ingall, 1994; Ingall and Jahnke, 1997). Changes in OM source or in primary production rates, as well as variations in basin circulation (i.e., downward advection of O_2 and upwelling of respired CO_2), may result in variations in the $\delta^{13}C$ composition of preserved bulk OM (Scholle and Arthur, 1980; Kump and Arthur, 1999) or in individual organic compounds (Hayes et al., 1987, 1990).

limiting nutrients (Murphy et al., 2000b). For this reason, the study is included in a volume on ‘‘Isotopic Records of Microbially Mediated Processes,’’ even though isotopic data comprise only one source of information in our multi-proxy reconstruction of organic matter burial.

2. Geological background

The stratigraphy of Middle–Upper Devonian rocks of the eastern United States has been extensively studied for many decades. Detailed lithic correlations extend from proximal facies of the Catskill delta

(eastern New York), through the axial part of the basin, across the peripheral bulge (e.g., Cincinnati Arch), and into the cratonic basin of western Kentucky and southern Indiana/Illinois (Ettensohn, 1985a,b; Ettensohn et al., 1988; Woodrow et al., 1988). Dominant marine lithofacies in the eastern part of this region (i.e., central to western New York representing the Appalachian foredeep to peripheral bulge) consist of medium gray to gray burrowed mudstones. Interbedded with the dominant mudstones are silty mudstone, siltstone, and sandstone intervals, interpreted to reflect regional shallowing, and finely laminated, dark gray to black, organic carbon-rich clay shales or mudstones, commonly associated with thin beds of skeletal carbonate and interpreted to reflect relative deepening (Ettensohn, 1985a,b; Ettensohn et al., 1988; Woodrow et al., 1988).

In this study, data were collected from six black mudstone units spanning latest Eilfelian through earliest Famennian time at two locations representing the distal part of the Appalachian foreland basin (Figs. 3 and 4). Earlier publications have described the geologic background for this study area in depth (Murphy et al., 2000a,b; Werne et al., 2002), and only the most pertinent aspects will be reviewed here. The black mudstones studied in detail include those of the Marcellus subgroup, the Geneseo, Middlesex, and Rhinestreet formations, as well as the Pipe Creek Formation and an interval of organic-rich facies in the uppermost Hanover Formation that together correspond to the lower and upper Kellwasser horizons (Murphy et al., 2000c) (Figs. 3 and 4). Each of these organic-rich intervals has been interpreted to coincide with a relative deepening event based on biostrati-

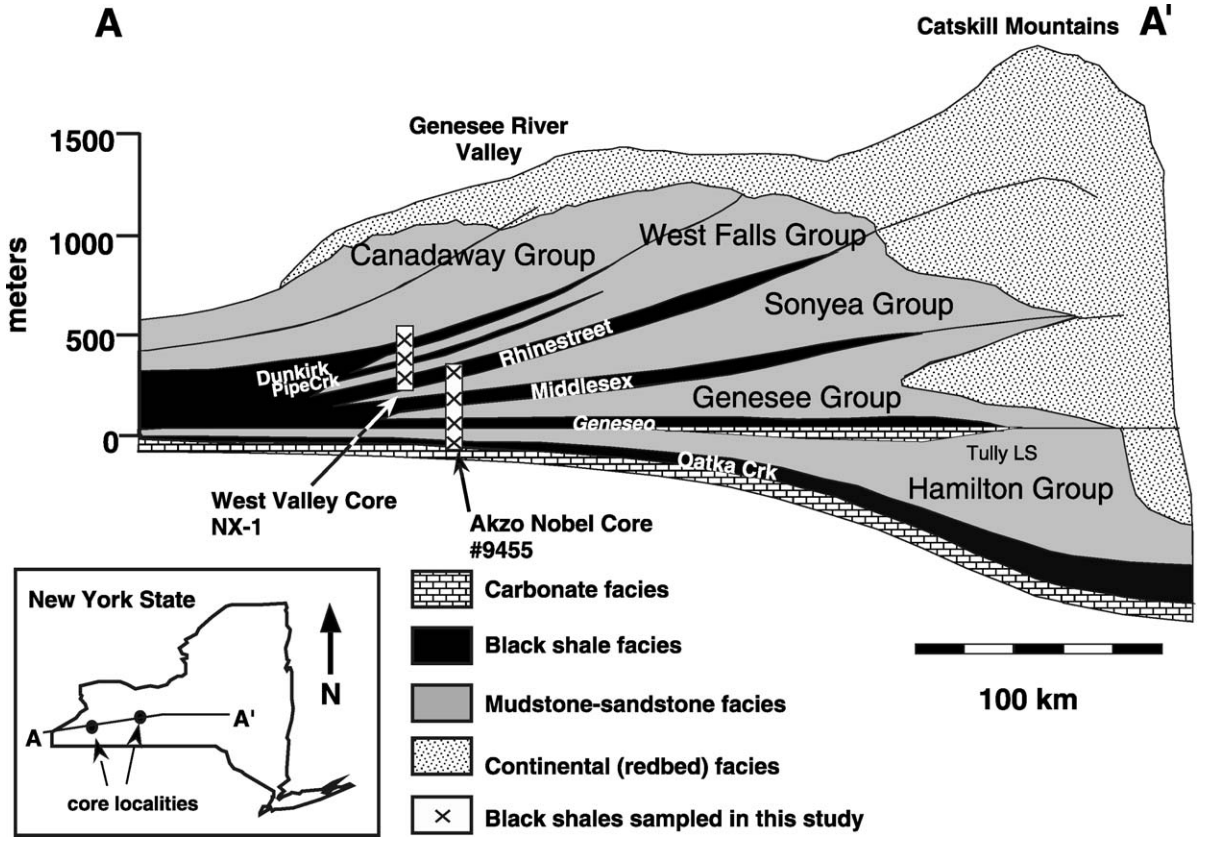

Fig. 3. Schematic cross section (A–A′) of the Catskill Delta Complex in New York (see inset map) showing core locations relative to major facies (modified from House and Kirchgasser, 1993).

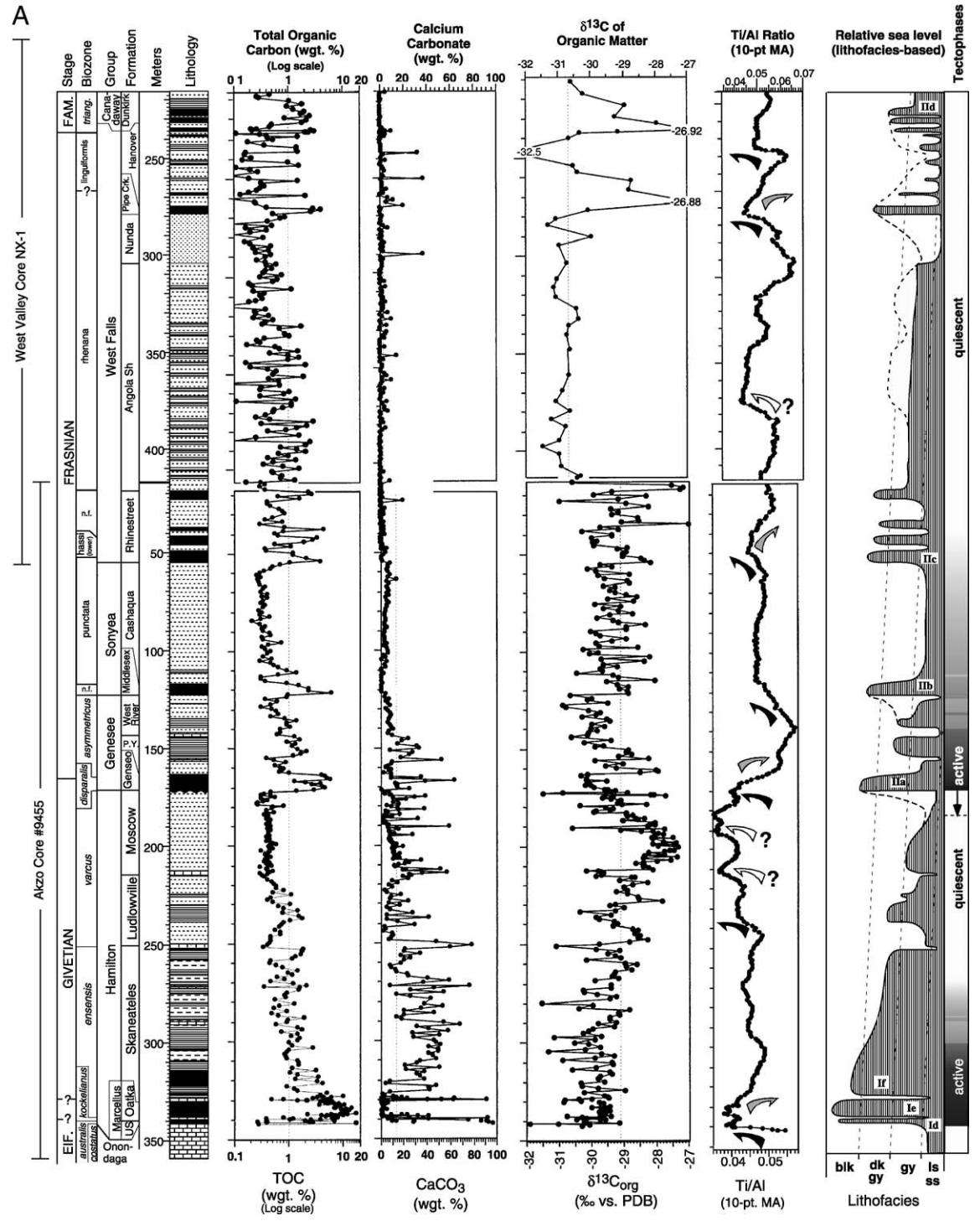
A
West Valley Core NX-1
Akzo Core #9455
Stage
Biozone
Group
Formation
Meters
Lithology
FAM.
FRASNIAN
GIVETIAN
EIF.
triang.
rhenana
ensensis
varcus
australis
kockelianus
costatus
Canadaway
Dunkirk
Hanover
Pipe Crk.
Nunda
Angola Sh
West Falls
Sonyea
Genesee
Hamilton
Marcellus
Onondaga
Oatka
Skaneateles
Ludlowville
Moscow
Cashaqua
Middlesex
West River
Geneseo
Rhinestreet
Total Organic Carbon (wgt. %) (Log scale)
Calcium Carbonate (wgt. %)
δ13C of Organic Matter
Tl/Al Ratio (10-pt MA)
Relative sea level (lithofacies-based)
Tectophases
quiescent
active
IId
IIc
IIb
IIa
If
Ie
Id
-26.92
-26.88
-32.5
TOC (wgt. %) (Log scale)
CaCO3 (wgt. %)
δ13Corg (‰ vs. PDB)
Ti/Al (10-pt. MA)
Lithofacies
blk
dk gy
gy
ls
ss

B
quiescent
active
quiescent
quiescent
active
quiescent
b
a
PB
FD
PB
FD
TP III
TPII
TPI
b a
200 km
WV
AK
Devonian limit
NY
Orogen
Basin
Shelf
Terrestrial
Lithologic Key
Limestone
Black shale
Dk gray mudst
Sandstone
Gray mudst
Marlstone
Limestone concretion

graphic correlation to proposed global eustatic events (i.e., Johnson and Sandberg, 1988), as well as regional sea-level reconstructions based on lithofacies and stratigraphic architecture (Brett, 1995; Brett and Baird, 1986; House and Kirchgasser, 1993; Ver Straeten and Brett, 1995) (Figs. 3 and 4). These deepening events may be related to the evolution of the Appalachian basin as suggested by Ettensohn (1985a,b) and Ettensohn et al. (1988). These papers present a tectono-stratigraphic model in which an active orogenic phase led to rapid subsidence in the foreland basin and black mudstone deposition. Subsequently, during the tectonic quiescence phase, erosion of the orogen resulted in basin filling with dark gray to gray mudstones until the terrigneous flux was reduced enough to allow carbonate platform development (Figs. 3 and 4). This subsidence model explains many patterns of sedimentation in the Eifelian through early Frasnian part of the section, but evidence discussed in Werne et al. (2002) suggests that eustasy also played a key role in basin history, especially for the post-Geneseo black mudstones. The long-term relationship between sea-level, terrigenous supply to the basin, and OM burial is illustrated in Fig. 4, with plots of weight percent total organic carbon (TOC), a 10-point moving average of Ti/Al ratio, and a composite relative sea-level curve.

The current consensus on paleogeography for the study interval places the basin at approximately 30–35° south of the equator (Witzke and Heckel, 1988; van der Voo, 1993; Scotese and McKerrow, 1990). The mid- to Late Devonian corresponds to the latter part of the Paleozoic greenhouse based on Berner's (1990) estimate of 4–12 times present-day pCO_2 values. Therefore, the basin probably lay within an expanded subtropical zone. Paleoclimatic indicators suggest warm but seasonally variable, arid to semi-arid conditions subject to significant storm activity (Woodrow et al., 1973; Heckel and Witzke, 1979; Scotese et al., 1985; Woodrow, 1985; Witzke and Heckel, 1988). This setting is consistent with sedimentologic evidence of storm wave base in the basin (e.g., Brett et al., 1986; McCollum, 1988; Prave et al., 1996; Schieber, 1999). Numerous lines of evidence suggest that climate cooled during the mid- to Late Devonian (Scotese and McKerrow, 1990; Copper, 1986; Buggisch, 1991; Isaacson et al., 1997). This trend is important insofar as it would have increased seasonal differences in evaporation/precipitation and surface-water temperature. In modern subtropical to temperate oceans, the warm season is characterized by a thin mixed layer and shallow thermocline (~ 20–40 m). During the cool season, as the frequency and intensity of mixing increases and water densities change, the mixed layer can expand to depths of over 140 m, and depending on the relative temperatures of the deep and surface layers, the thermocline may dissipate altogether.

The importance of thermal stratification in the marine oxygen budget has long been recognized (e.g., Fleming and Revelle, 1939) and was recently reviewed in a volume on continental shelf anoxia (Tyson and Pearson, 1991). Because the Appalachian basin was most likely at shelfal depths for much of its history and had open connections to the global Devonian ocean, the establishment and breakdown of seasonal thermoclines should be considered as an alternative to the conventional "nearly permanent" pycnocline model (Ettensohn, 1985a,b).

Fig. 4. Overview of data for Akzo and West Valley cores includes lithology (based on high-resolution core descriptions), TOC (dashed line shows 1% level separating gray from dark gray and black mudstones), $CaCO_3$, $\delta^{13}C_{org}$, Ti/Al ratio (10-point moving average; black arrows = decrease in Ti/Al associated with TOC increase; gray arrows = increase in Ti/Al associated with TOC decrease; white arrows = no correlation), and interpreted relative sea-level curve. Lithostratigraphy and biostratigraphy follow Rickard (1975), House and Kirchgasser (1993), Kirchgasser et al. (1994), Ver Straeten et al. (1994), and Klapper and Becker (1999); sea-level curve is based on combination of lithofacies (House and Kirchgasser, 1993; Brett and Baird, 1996), trends in $CaCO_3$ and Ti/Al, and regional stratigraphy (Fig. 3), and includes labels for correlative eustatic events of Johnson and Sandberg (1988). Tectophases of Ettensohn (1985a,b) are shown next to sea-level curve (note possible re-interpretation of Tectophase II initiation based on Ti/Al data), and are illustrated (facing page) in a series of cross-sectional cartoons (based on Ver Straeten, Devonian paleogeographic map of New York State illustrates three major hypsometric zones (terrestrial, shelfal, basinal), and highlights the interpreted expansion of the shelfal zone during relative sea-level fall and basin filling (modified from Dennison, 1985; McGhee and Sutton, 1985); note correlation of positions "a" and "b" in tectophase cartoons and paleogeographic map. N.F. = no fossils; US = Union Springs Member of Bakoven Formation; PY = Penn Yan Formation. Lithologic key applies to Figs. 4–10.

3. Materials and proxy methods

The data presented herein include geochemical analyses of samples from two cores drilled in western New York. Akzo core #9455 (donated by the Akzo Nobel Salt) was drilled in the Genesee valley, Livingston, NY, and includes the interval from the Onondaga Limestone through the Rhinestreet Shale (Figs. 3 and 4). West Valley core NX-1 (loaned for sampling by the New York State Geological Survey) was drilled some 50 miles west of the Akzo site, in Cattaraugus, NY, and includes the interval from the Rhinestreet Shale through the Dunkirk Formation (Figs. 3 and 4). Together, these cores preserve a pristine record of latest Eifelian through earliest Famennian strata.

Each core was measured and described at mm- to cm-scale for lithologic, sedimentologic, and paleontologic observations (e.g., rock color, lithology, sedimentary structures, ichnofabric and ichnotaxa, and identifiable macrofossils). Subsamples for geochemistry and petrography were cut from the cores at 1-m spacing throughout (Fig. 4), and at 10–20 cm spacing in the intervals spanning black mudstones (Figs. 5–10). Thin sections were analyzed using standard petrographic techniques, and selected sections were examined under scanning electron microscope for grain textures and surface features. Selected subsamples were analyzed commercially for organic petrography using standard methods of maceral preparation and identification (Durand, 1980; Stach et al., 1982); point counting yielded quantification of two major classes of identifiable kerogen elements (macerals): (1) amorphous, fluorescent liptinite–vitrinite, characteristic of algal-derived OM, and (2) vitrinite–inertinite, a nonfluorescent, highly structured, optically opaque maceral representing cellulose-rich, woody and herbaceous materials derived from land plants.

Geochemical proxies for production, dilution, and microbial decomposition are based on elemental and isotopic data as explained in Fig. 2. More detailed discussion of these proxy methods, as well as descriptions of sample preparation and analytical techniques for each method can be found in Murphy et al. (2000a,b), Werne et al. (2002), and references therein.

4. Results and discussion

One of the key contributions of the large geochemical database developed in this project is the establishment of proxy baselines against which relative trends can be assessed. Table 1 summarizes values for the mean and one standard deviation of proxy data in samples with TOC content less than 1 wt.%. These samples correspond to the gray shale facies of Brett et al. (1991) interpreted to represent deposition under normal marine, well-oxygenated conditions, and thus represent "continental" values for metals and other elements. Hereafter, these values will be referred to as "GSM" (gray shale mean) or "1σ-GSM" (one standard deviation of the gray shale mean). In Figs. 5–10, proxy data are shown relative to GSM with shading for 1σ-GSM so that the extent of

Table 1
Gray shale mean (GSM) and one standard deviation for selected proxies in mudrock samples with %TOC ≤ 1 (limestones excluded) from the Akzo and West Valley cores, respectively

		TOC	$CaCO_3$	Ti/Al	Si/Al	Mo	V + Cr	Mn	$\delta^{34}S$	$\delta^{13}C$	C_{org}/N_{tot}	C_{org}/P_{tot}
Akzo	Mean	0.5	13.63	0.045	3.14	0.22	203.6	419.1	−9.05	−29.1	6.6	25
	σ	0.18	15.3	0.0059	0.36	1.06	48.9	120.7	10.19	0.89		
	N	227	227	227	227	227	227	223	23	227		
West Valley	Mean	0.45	3.5	0.054	4.24	0.96	210.5	444.9	−9.05	−30.6	6.6	25
	σ	0.26	5.6	0.0081	1.28	2.35	58.5	152.5	10.19	0.58		
	N	141	141	141	141	141	141	138	23	17		

Mean C_{org}/N_{tot} values for efficiently buried (gray shale) OM based on modern Redfield ratio. Mean C_{org}/P_{tot} based on averages from gray mudstones with $C_{org}/P_{org} = \pm$ Redfield (106). DOP values, where available, are shown with dysoxic–oxic boundary (0.45) and dysoxic–anoxic boundary (0.75) based on Raiswell et al. (1988).

anomalies from background continental or "oxic" conditions can be quantified and compared. Note that baseline values are calculated separately for the Akzo and West Valley cores. The difference in some mean proxy values between the cores (in particular, $CaCO_3$, Ti/Al, Si/Al) is interpreted to reflect a secular shift in dilution related to westward progradation of the Catskill Delta complex.

4.1. Marcellus subgroup

The Marcellus subgroup (Ver Straeten et al., 1994) conformably overlies the Seneca member of the Onondaga Limestone in the study area and includes (Fig. 5): the 30-cm Bakoven member of the Union Springs Formation, a highly organic-rich, black calcareous mudstone–marlstone with interlaminated skeletal lags composed of abundant styliolinids and fragments of rhynchonellid brachiopods; the 10-cm Hurley member, a medium gray concretionary, micritic limestone horizon that is bioturbated and contains abundant crinoid and styliolinid debris; and four informal members of the Oatka Creek Formation. These informal members include (Fig. 5): (1) the 35-cm bioclastic Cherry Valley Limestone, a medium-gray packstone composed dominantly of skeletal debris from styliolinids, corals, brachiopods, and crinoids (incised into the Hurley member); (2) the 170-cm Berne member, a medium dark gray, organic-rich mudstone with poorly laminated to burrowed horizons, styliolinid debris, and small brachiopods and bivalves; (3) the 45-cm Halihan Hill bed, a highly bioturbated bioclastic limestone with abundant styliolinids and macrofauna including brachiopods, bryozoans, small bivalves and gastropods; and (4) the ~ 9-m-thick unnamed member, a highly organic-rich, laminated silty mudstone with scattered styliolinids and fish debris. The Marcellus subgroup is overlain by the basal Stafford Limestone member and dark gray mudstones of the Skaneateles Formation (Figs. 4 and 5).

Framboidal and euhedral pyrite occur throughout the laminated organic-rich facies, and the upper contacts of limestones overlain by organic-rich mudstones are commonly pyritized hardgrounds (Ver Straeten et al., 1994). Most contacts in the Marcellus subgroup are relatively sharp, but the boundary between the Hurley member and the Cherry Valley Limestone is quite irregular and shows evidence of incision. Regional observations indicate an erosional unconformity at this contact (Ver Straeten et al., 1994). The biostratigraphy of the Marcellus subgroup is not very well resolved (Ver Straeten et al., 1994); representatives of late Eifelian and early Givetian conodont and ammonoid biozones have been identified within the interval (e.g., Klapper, 1971, 1981; House, 1981), but the exact placement of the Eifelian–Givetian boundary remains unclear. These observations reflect a relative degree of conformity through the interval (e.g., conodont biozones *australis* and *kockelianus* are 0.6–0.7 my in duration according to the Tucker et al., 1998 timescale, therefore the lacuna associated with the Cherry Valley unconformity is probably relatively small), but they also suggest significant condensation.

The Oatka Creek Formation was recently described and analyzed in detail by Werne et al. (2002), and the Union Springs Formation was investigated by Murphy (2000). As shown in Figs. 4 and 5, these two units have the highest TOC content recorded in this entire study, with values up to ~ 18%. At the time of Marcellus subgroup deposition, the Akzo core site was as much as 400 km from the eastern shoreline of the basin (Dennison, 1985), and the depth of the basin depocenter is estimated to have been in excess of 150 m by Ettensohn (1985a).

4.1.1. Dilution/condensation

The 10-point moving average of Ti/Al in Fig. 4 shows a distinctive decrease associated with Marcellus subgroup black mudstones and a subsequent increase in the overlying dark gray to gray mudrocks of the Skaneateles Formation, suggesting that siliciclastic sediment starvation is associated with OC enrichment. The detailed data in Fig. 5 show that Ti/Al ratios in most samples of the Marcellus subgroup are below the GSM for the Akzo core, but there are some notable exceptions. For example, the Cherry Valley Limestone–Hurley member shows the highest Ti/Al value recorded in the entire data set, which is clearly the cause of the elevated values in the basal points of the moving average calculation. The base of the Cherry Valley Limestone is incised and has been interpreted to reflect an unconformity formed during a lowstand between the relative sea-level rise events that deposited the Union Springs and Oatka Creek

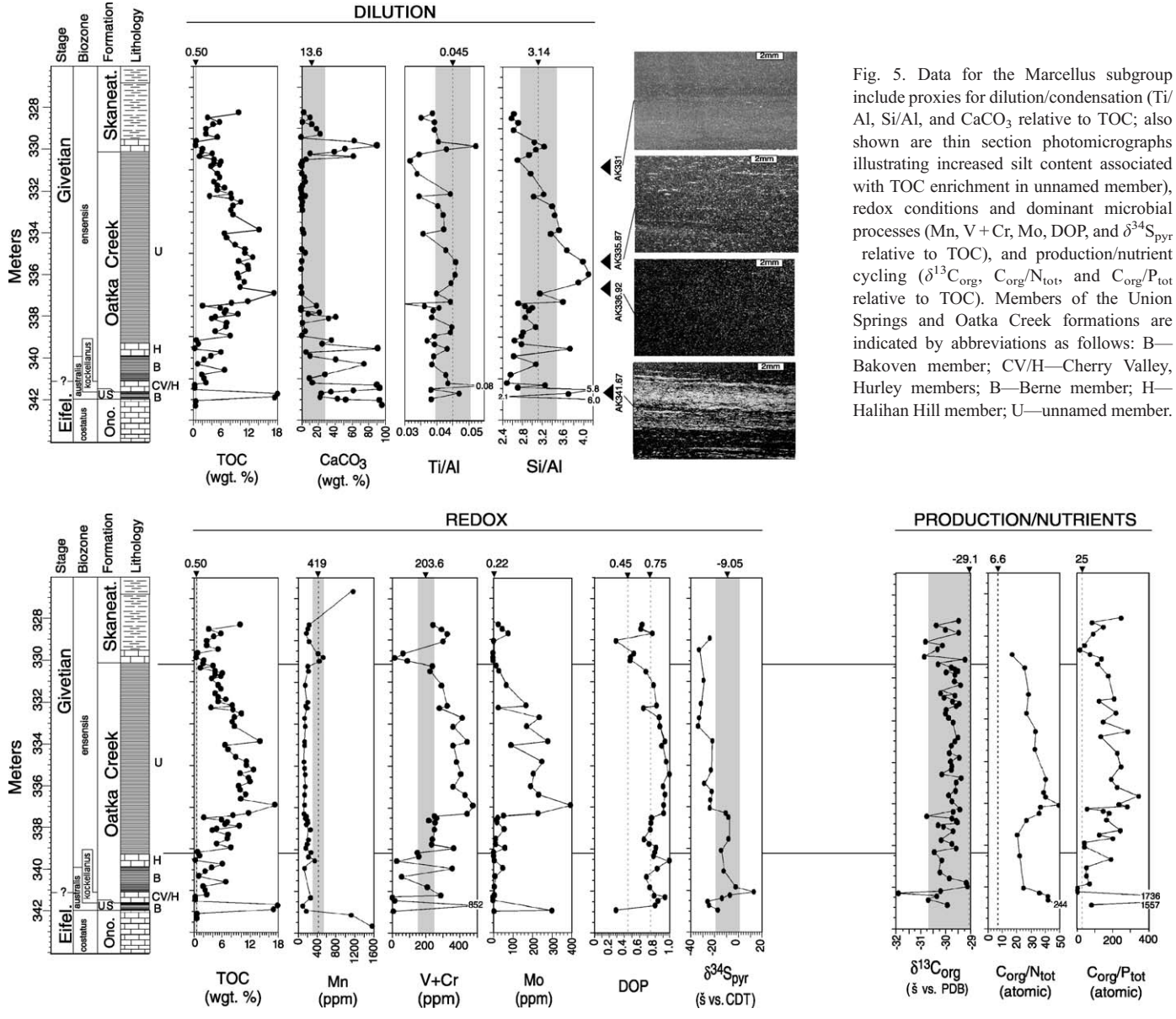

Fig. 5. Data for the Marcellus subgroup include proxies for dilution/condensation (Ti/Al, Si/Al, and $CaCO_3$ relative to TOC; also shown are thin section photomicrographs illustrating increased silt content associated with TOC enrichment in unnamed member), redox conditions and dominant microbial processes (Mn, V + Cr, Mo, DOP, and $\delta^{34}S_{pyr}$ relative to TOC), and production/nutrient cycling ($\delta^{13}C_{org}$, C_{org}/N_{tot}, and C_{org}/P_{tot} relative to TOC). Members of the Union Springs and Oatka Creek formations are indicated by abbreviations as follows: B—Bakoven member; CV/H—Cherry Valley, Hurley members; B—Berne member; H—Halihan Hill member; U—unnamed member.

formations (i.e., between eustatic events Id and Ie, Fig. 4).

Another characteristic that is inconsistent with the bulk of observations in this study is the pattern of Ti/Al within the unnamed member. Although the lowest Ti/Al value in this interval coincides with a shift to maximum TOC levels (where there are no changes in lithology or sedimentary structures), Ti/Al values do not remain low through this interval. An explanation may be found in the Si/Al data. In contrast to Ti/Al, the Si/Al ratio tracks TOC enrichment quite well, showing significant increases above GSM in the unnamed member, and some of the highest values recorded in the study occur within the Bakoven member (Fig. 5). Observations of thin section photomicrographs show dense concentrations of styliolinids along laminae of the Bakoven member and maximum silt concentrations occur in the zone of maximum TOC of the unnamed member (Fig. 5). SEM photomicrographs reveal these silt grains to be subangular, and some show pitted surface textures, suggesting eolian origin. Based on these observations, Werne et al. (2002) argued that the concentration of eolian silt grains became enriched due to decrease in the flux of non-eolian siliciclastic and carbonate sediment. Therefore, maximum TOC enrichment correlates with maximum sediment starvation. In addition to the quartz silt, grains bearing Ti may also have been transported to the basin by eolian processes (Bertrand et al., 1996), a factor that could explain why Ti/Al does not remain at minimum values through the zone of maximum TOC in the unnamed member.

The high concentration of styliolinids in the Bakoven member probably reflects the same mechanism, although their low abundance in the unnamed member suggests significant differences between the two units. Differential preservation of carbonate might explain this relationship, but the scattered styliolinids of the unnamed member do not show signs of dissolution, and redox indicators (described below) suggest conditions were similar during deposition of the two units (both anoxic–sulfidic). An alternate explanation is that ecological differences prevented styliolinids from flourishing during deposition of the unnamed member (styliolinids are interpreted to represent protist zooplankton; Yochelson and Lindemann, 1986). The basinal depocenter for the Bakoven member is much farther east than that of the Oatka Creek Formation (Pepper and de Witt, 1951). As a result, the Akzo site may have been closer to the western peripheral bulge of the basin and therefore shallower during Bakoven deposition.

4.1.2. Decomposition/redox state

Although OC concentrations achieve peak values in the intervals for which there is evidence of maximum condensation, TOC levels are relatively high throughout the Marcellus subgroup. The role played by preservation in this high burial flux is indicated by selected redox-sensitive elements. For example, Mn concentrations are quite high in the upper Onodaga Limestone (>1000 ppm), most likely due to the preferential incorporation of Mn in the carbonate lattice under oxic conditions. Mn values fall to ± 200 ppm throughout the Marcellus subgroup, a level significantly below the GSM for Mn (Fig. 5). This suggests that oxygen deficiency dominated during Marcellus deposition. The degree of oxygen deficiency is indicated by the remaining proxies.

The V + Cr proxy is significantly elevated above GSM in the Bakoven member and the zone of maximum starvation of the unnamed member. It has been suggested that enrichment in V + Cr could indicate oscillation of redox conditions in the water column and sediment through the zone of denitrification (suboxic). The strong correlation of V + Cr with indicators of condensation in the unnamed member also suggests there may be a sedimentation effect. However, the fact that V + Cr is even more enriched in the Bakoven member, interpreted to have been deposited further up the western ramp than in the basin depocenter, may be consistent with the hypothesis of oscillating redox conditions, since a shallower site would have been subject to more frequent water column disturbance.

DOP is elevated throughout the Marcellus subgroup to levels suggesting lower dysoxic to anoxic conditions (Raiswell et al., 1988), but again it is difficult to separate the effects of sedimentation rate from redox controls, especially since variations in the overall high DOP values closely track the zones of maximum starvation. The enrichment of Mo within the Bakoven and unnamed members shows one of

the most marked deviations from GSM values, and although condensation is also implicated in this pattern, anoxic–sulfidic conditions are required for Mo accumulation (e.g., Emerson and Huested, 1991; Dean et al., 1999; Lyons et al., 2002, this volume). This conclusion is confirmed finally by the $\delta^{34}S_{pyr}$ data, which show values depleted to <-25‰ in the Bakoven member and to almost -40‰ in the unnamed member, suggesting open system (water column) pyrite formation (Lyons, 1997). Interestingly, the maximum depletion in $\delta^{34}S_{pyr}$ occurs as TOC and Mo values are declining in the uppermost samples of the unnamed member due to increased bulk sedimentation.

4.1.3. Production/nutrient cycling

Petrographic analysis of preserved OM in one sample of Marcellus subgroup black mudstones indicated 100% amorphous marine material among the macerals with trace palynomorphs as accessories. Organic compound analyses of the distributions and relative abundances of short- (15, 17, and 19 carbons) and long-chain (27, 29, and 31 carbons) *n*-alkanes in the Seneca, Bakoven, Hurley–Cherry Valley, and lowermost Berne members indicate that short alkanes are consistently an order of magnitude more abundant than long ones in organic-rich facies; the reverse is true for the carbonate facies (Murphy, 2000). These observations, suggesting increased terrestrial organic matter supply to the basin during limestone deposition and algal predominance over terrestrial input in the preserved organic matter of the black mudstone facies, are consistent with the interpreted sea-level history (Fig. 4). Because organic matter input during mudstone deposition was predominantly derived from marine phytoplankton, it is assumed its original elemental composition approximated the marine Redfield ratio (Redfield et al., 1963).

With the exception of a few samples in the Hurley–Cherry Valley carbonates, the carbon isotopic composition of bulk organic matter varies by 1‰ or less around a mean value of -30‰ throughout the Marcellus subgroup and shows no trend that is correlative with other proxies (Fig. 5). This mean value is slightly depleted relative to GSM for $\delta^{13}C_{org}$ in the Akzo core (-29.1‰), but the GSM value is clearly influenced by samples overlying the Hamilton Group, as well as those of the Moscow Formation, which are relatively enriched in ^{13}C (Fig. 4). In fact, despite high-frequency variability associated with facies changes, the average value of $\delta^{13}C_{org}$ for mudstones in the lower Hamilton Group (Marcellus subgroup and Skaneateles Formation) does not show a major secular trend. Although the range of sample-to-sample variation increases markedly in the units overlying the Oatka Creek Formation (Fig. 4), the C-isotope composition of organic matter in Marcellus subgroup black mudstones is essentially identical within error.

The ratio of carbon to nitrogen (C_{org}/N_{tot}) in OM is quite high in the limestone facies (>200), which is consistent with a higher proportion of terrestrial OM and/or extensive decomposition of more labile marine OM. Average C_{org}/N_{tot} values in the black mudstones range between 30 and 50, with the highest values corresponding to the zones of maximum TOC enrichment. These values are five to seven times greater than the Redfield ratio. Within the unnamed member, C_{org}/N_{tot} correlates well with TOC, V + Cr, and Mo. The ratio of TOC to total phosphorous (C_{org}/P_{tot}) is used rather than C_{org}/P_{org} (Van Cappellen and Ingall, 1994) because remineralized P is not necessarily released to the overlying water column, but may instead become immobilized in sediments in inorganic form (e.g., Fillipelli, 1997). Thus, the C_{org}/P_{tot} ratio provides a conservative estimate of remineralized P. It shows a pattern of enrichment similar to C_{org}/N_{tot} in the black mudstone facies, with values in excess of 1500 in the Bakoven and levels of over 200 in the unnamed member. According to Table 1, the GSM for C_{org}/P_{tot} is ~ 25. This value is derived as follows: OM in gray mudstones was probably relatively rapidly buried and thus likely experienced the lowest levels of P remineralization (a test of H/C ratios confirmed this, showing greater H-richness in gray mudstone samples). Therefore, it is likely that the C_{org}/P_{org} values of gray mudstones reflect the most well-preserved primary organic matter in the study. The C_{org}/P_{org} of such samples is almost identical to the Redfield value (± 106), and the corresponding value for C_{org}/P_{tot} in these samples is ~ 25. Values of C_{org}/P_{tot} in the unnamed member are approximately 10 times greater than this value, and 60–70 times higher in the Bakoven.

4.1.4. Summary

The entire Marcellus subgroup appears to be condensed relative to gray mudstone in the Akzo core. The close correspondence between maximum TOC enrichment and evidence for maximum starvation without any other changes in lithology in the core of the unnamed member suggest that this zone represents the maximum flooding surface of sea-level rise event Ie (Johnson and Sandberg, 1988). Thus, the decrease in bulk sedimentation (including the complete shut down of carbonate) probably played a significant role in TOC enrichment (Werne et al., 2002). The degree to which excess Si in the zone of maximum TOC enrichment is attributable to biogenic production (i.e., Schieber et al., 2000) is not known, although observations thus far suggest that eolian silt is a significant factor. Although C/N/P elemental data suggest decompositional release of nutrients from OM, there is no isotopic evidence for enhanced production in the Marcellus subgroup black mudstones. The redox-sensitive proxies, however, indicate that anoxic conditions dominated during deposition of the Marcellus subgroup, with euxinic conditions a common occurrence in the Bakoven member and unnamed member of the Oatka Creek Formation.

4.2. Geneseo Formation

The Geneseo Formation is an approximately 8-m-thick black, finely laminated, organic-rich, mudrock with several marlstone beds in the upper half (Fig. 6). It is similar in its general lithic and faunal character to the black mudstones of the Marcellus subgroup. Unlike the Marcellus, however, it is slightly calcareous throughout and does not achieve even half the TOC values seen in the Bakoven member or Oatka Creek Formation. Two peaks in TOC content to about 6% in the lower and upper parts of the unit are separated by a zone of increased carbonate content with two marlstone beds. The mudrocks contain common styliolinids and scattered thin *Leiorhynchus* shells, as well as euhedral and framboidal pyrite.

In the region from the Genesee Valley to the west, the Geneseo Formation is underlain by gray mudstones of the Windom member, Moscow Formation, and overlain by gray mudstones of the Penn Yan Formation. At the Windom–Geneseo contact, there is a major unconformity represented by the Leicester Pyrite, a ±10-cm-thick reworked lag deposit of pyritized skeletal fragments and burrow casts (Brett and Baird, 1996). To the east this unconformity expands to include the Tully Limestone, which represents carbonate platform deposition at the end of Tectophase II (Fig. 4). Following Tully deposition, the Geneseo Formation was deposited during the Taghanic sea-level rise (event IIa, Fig. 4) that initiated Tectophase III and is therefore analogous to the Marcellus subgroup in the Ettensohn (1985a,b) tectono-stratigraphic model. At the time of deposition, the Akzo core site was at least 250 km from the eastern shoreline (Brett and Baird, 1996), and water depths are estimated to have been over 200 m (Ettensohn, 1985a). The Geneseo corresponds to the *disparalis* biozone; based on both conodont and goniatite biostratigraphy (Kirchgasser et al., 1994) the Givetian–Frasnian stage boundary is placed at the upper contact. According to the recent Tucker et al. (1998) timescale, the Geneseo represents ~1 my of deposition. The Geneseo Formation was recently described and analyzed in detail by Murphy et al. (2000b).

4.2.1. Dilution/condensation

The long-term trend in Ti/Al shows a minimum value in the upper Windom member and then a secular increase in Ti relative to Al across the Givetian–Frasnian boundary and through the Genesee Group (Fig. 4). This increase is interrupted at the base of the Geneseo, where Ti/Al values drop before continuing to rise. The detailed data in Fig. 6 show that Ti/Al is below GSM for the Akzo core through most of the Geneseo, has a weakly inverse relationship with %TOC, and gradually rises above the GSM by the end of Geneseo deposition. With the exception of the mid-Geneseo, the Si/Al ratio tracks the long-term trend in Ti/Al. For example, Si/Al data show an increase from below GSM in the lower Geneseo to anomalously high values in association with mid-Geneseo marls (Fig. 6). Ratios of Si/Al return to sub-GSM levels in the upper part of the unit before they resume tracking the rise in Ti/Al in the lower Penn Yan Formation. Thin section photomicrographs confirm the presence of quartz silt in the middle Genseso, but unlike the Marcellus subgroup, this zone is

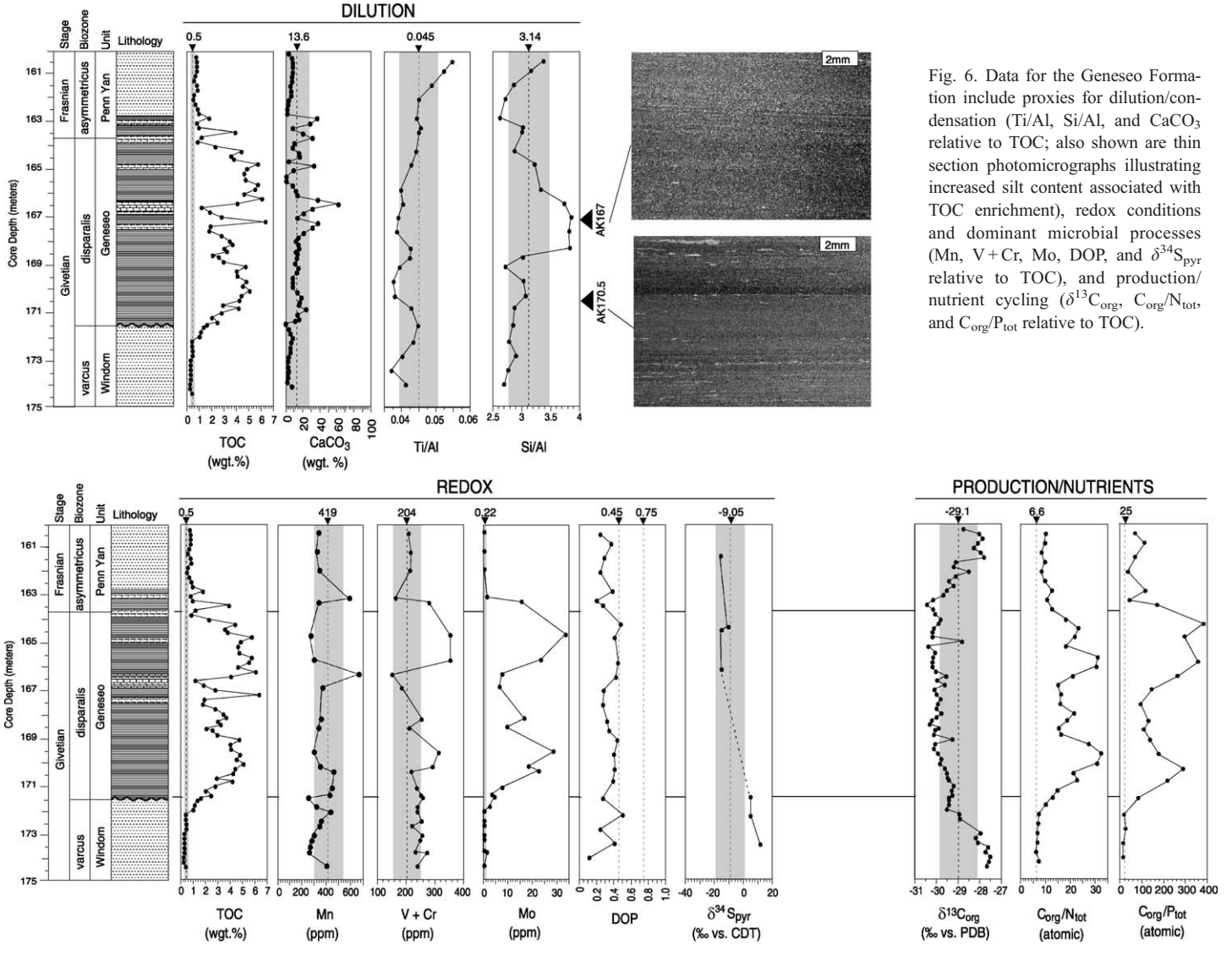

Fig. 6. Data for the Geneseo Formation include proxies for dilution/condensation (Ti/Al, Si/Al, and $CaCO_3$ relative to TOC; also shown are thin section photomicrographs illustrating increased silt content associated with TOC enrichment), redox conditions and dominant microbial processes (Mn, V + Cr, Mo, DOP, and $\delta^{34}S_{pyr}$ relative to TOC), and production/nutrient cycling ($\delta^{13}C_{org}$, C_{org}/N_{tot}, and C_{org}/P_{tot} relative to TOC).

characterized by a decrease in %TOC rather than an increase. Carbonate appears to act as a minor dilutant in the upper half of the Geneseo, where it varies antithetically with %TOC.

4.2.2. Decomposition/redox state

Concentrations of redox-sensitive proxies suggest oxygen deficiency during deposition of the Geneseo Formation, but to a much lesser degree than the Marcellus subgroup. For example, Mn concentrations are below GSM through most of the interval shown in Fig. 6 (with the exception of burrowed marlstone beds), but they only rarely exceed the range of 1σ-GSM. If depletion in Mn is a function of duration of anoxia (Calvert and Pedersen, 1996), these data suggest that anoxic conditions were relatively short-lived. Levels of V + Cr are slightly above GSM in the upper Windom and lower Geneseo, but show marked enrichment in association with the zones of maximum TOC (Fig. 6), where they vary antithetically with Mn. A similar pattern of enrichment is seen in the Mo data but the maximum values are ~ 30 ppm (~ 10 times less than maximum Mo values in the Marcellus subgroup). Values for DOP are consistently lower than the 0.45 level, suggesting pervasively oxic conditions or rapid siliciclastic sedimentation under euxinic conditions. Although pyrite sulfur isotope values are depleted in the Geneseo relative to the Windom member, no measured values exceeded 1σ-GSM for $\delta^{34}S_{pyr}$. Together, these data indicate that anoxic–sulfidic conditions did occur during Geneseo deposition but with much lower frequency and/or duration than during Marcellus time. The mean condition was probably closer to suboxic.

4.2.3. Production/nutrient cycling

Petrographic analysis of preserved OM in a sample of Geneseo black mudstones indicated 100% amorphous kerogen in the macerals with trace palynomorph accessories, suggesting dominance of marine OM. Similar analyses of Moscow and Penn Yan gray mudstones showed 95% amorphous kerogen with about 5% structured woody material in the macerals. Molecular analyses of the distribution/relative abundance of *n*-alkanes provide supporting data for distinguishing terrestrial and marine contributions. The combined abundances of C_{17} and C_{19} (normalized to total lipid extract) are assumed to represent the "marine" fraction compared to the combined, normalized abundances of C_{27} and C_{29}, assumed to represent the "terrigenous" fraction (Murphy, 2000). In the Geneseo black mudstones, there is a decrease in the terrestrial fraction, but more significant is the approximate 100% increase in the marine fraction (Murphy et al., 2000b). Thus, at the Akzo location, OM in both gray and black facies is most likely dominantly sourced from marine photoautotrophs, but there appears to have been a relative increase in the marine OM flux during Geneseo black mudstone deposition.

Among the most distinctive features of the Geneseo data set is the ~ 2‰ depletion in $\delta^{13}C_{org}$ values from about −28‰ to −30‰ associated with organic carbon accumulation (Fig. 6). This depletion appears to begin in the uppermost Windom and continues through most of the Geneseo Formation until values shift back to −28‰ in the Penn Yan Formation. The Geneseo is also characterized by significant shifts in the burial ratios of C/N/P. As shown in Fig. 6, C_{org}/N_{tot} shows a pattern very similar to that of %TOC, with values rising from Redfield levels of ~ 6 to ~ 30 in the lower and upper organic-rich zones (at least a fourfold increase). The pattern of C_{org}/P_{tot} is also correlated with changes in TOC but shows enrichment from Redfield equivalent levels of 25 to >300 (over 10 times Redfield level). Because of arguments discussed above showing that terrestrial OM did not increase in the organic-rich units, increase in the C_{org}/N_{tot} ratio must reflect elemental fractionation during pre-burial decomposition and early diagenesis.

4.2.4. Summary

Multi-proxy data for the black mudstones of the Geneseo Formation differ significantly from those of the Marcellus subgroup. Levels of TOC are enriched well above GSM, but are much lower than those of the Marcellus. Like the Oatka Creek Formation (Werne et al., 2002), there is little evidence of bioturbation in the Geneseo mudstones and only a sparse benthic fauna (cf. Thompson and Newton, 1987), but the geochemical evidence does not indicate euxinic depositional conditions. The critical question is whether these two intervals are analogous, as suggested by the Tectophase model.

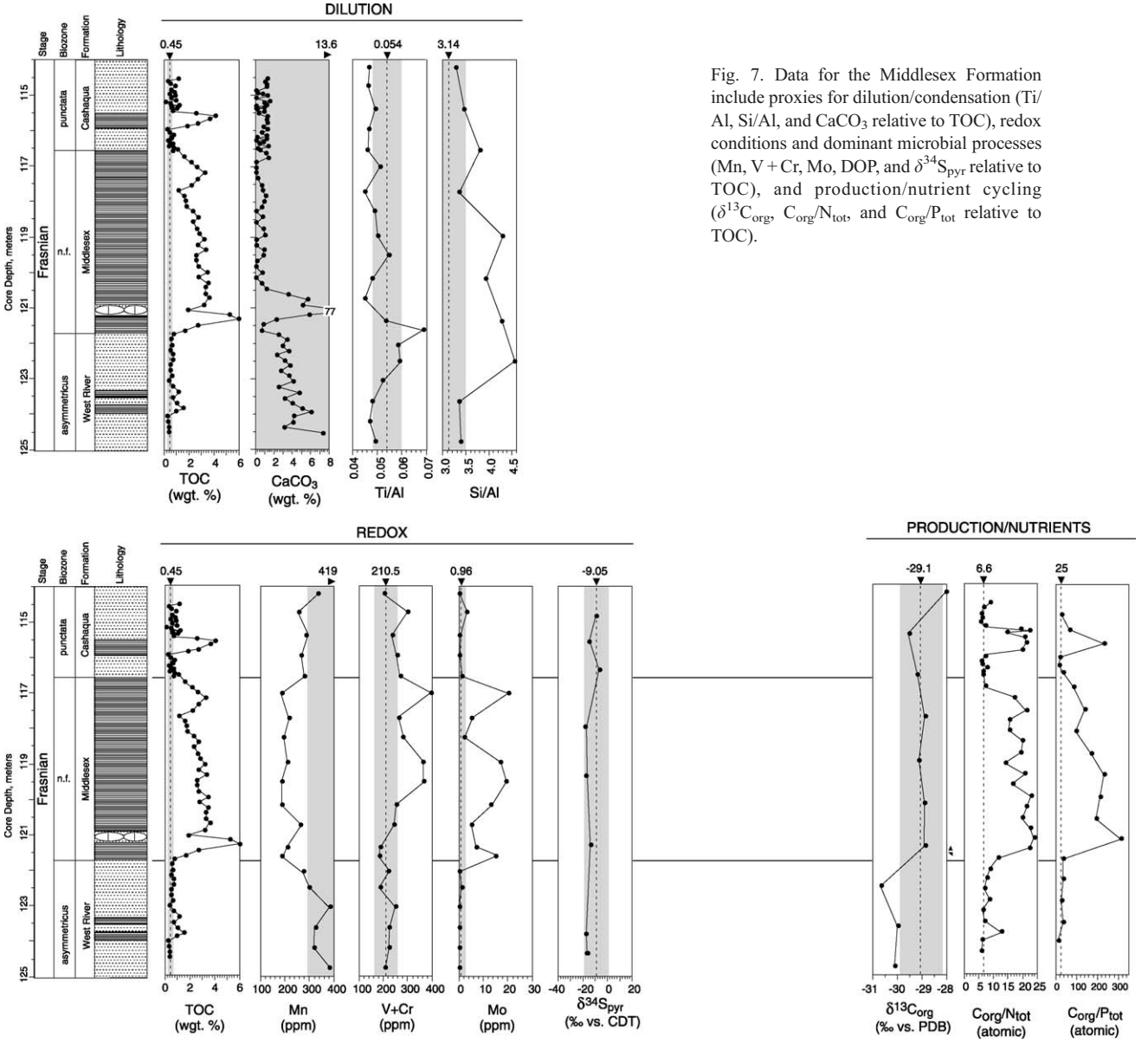

Fig. 7. Data for the Middlesex Formation include proxies for dilution/condensation (Ti/Al, Si/Al, and $CaCO_3$ relative to TOC), redox conditions and dominant microbial processes (Mn, V + Cr, Mo, DOP, and $\delta^{34}S_{pyr}$ relative to TOC), and production/nutrient cycling ($\delta^{13}C_{org}$, C_{org}/N_{tot}, and C_{org}/P_{tot} relative to TOC).

The first major difference between the Marcellus and the Geneseo manifests in sedimentation proxies. The general correspondence of decreased Ti/Al with increased TOC observed in most black shales in the study interval (Fig. 4) argues for a condensation effect in OM accumulation. However, there are nuances in the Ti/Al data. For example, the data in Fig. 6 show a correspondence between minimum Ti/Al levels and the initiation of enhanced OM accumulation at the base of the Geneseo Formation. Yet the record in Fig. 4 indicates that this pattern is a short-term fluctuation in a longer-term trend of increasing Ti/Al that actually begins in the Moscow Formation. Although short-term trends in Ti/Al appear to be consistent with a condensation interpretation, the longer-term trends need to be addressed: why does Ti/Al ratio reach its absolute minimum in the Moscow Formation, a late highstand (Brett and Baird, 1996) where one would expect siliciclastic flux to be highest, and then show an overall increase across the transition from Tectophase II to III which represents a major transgression? We address this question below in Section 5.

The interpretation of Si/Al ratio is another difference between the Marcellus and the Geneseo intervals. In the middle part of the Geneseo Formation, Si/Al increases to levels above 1σ-GSM, as it does in the unnamed member of the Oatka Creek Formation, but rather than correlating with a shift to maximum TOC values, there is a marked decrease in TOC (Fig. 6). At the onset of this Si/Al increase and TOC decrease, there is a small spike in the Ti/Al ratio followed by a return to values below 1σ-GSM. The Ti/Al decrease is concomitant with a rise in $CaCO_3$ values (Fig. 6), and is followed by a gradual increase in Ti/Al through the remainder of the unit (corresponding to basinward progradation of the shoreline). Increase in $CaCO_3$ levels was not observed in association with increased Si/Al in the Marcellus; however, a thin section photomicrograph from within the zone of elevated Si/Al shows an increase in the quartz silt fraction, just like the unnamed member of the Oatka Creek Formation. A possible explanation for the $CaCO_3$ and TOC trends is closer proximity to the western carbonate shelf during Geneseo deposition, resulting in a greater potential flux of $CaCO_3$ to the basin, and thus dilution of TOC by carbonate in the condensed beds of the maximum flooding interval. If the increase in Si/Al was due to excess biogenic Si as a result of a major increase in production (or a shift in community composition) at this time, one might also expect TOC levels to rise.

The final factor that differs markedly in the Geneseo data set manifest in the $\delta^{13}C_{org}$ data. While there is no clear trend exceeding 1σ-GSM for bulk $\delta^{13}C_{org}$ through the Marcellus subgroup, there is a definite negative shift of $\sim 2‰$ associated with OC burial in the Geneseo Formation (Fig. 6). Murphy et al. (2000b) explained this shift as a consequence of mixing isotopically light respired $CO_{2(aq)}$ into surface waters during seasonal mixing events (e.g., Saelen et al., 1998).

4.3. Middlesex, Rhinestreet, Pipe Creek, and Hanover formations

In the interval overlying the Geneseo Formation, there are four distinct zones of OC enrichment with characteristics that are similar to one another and distinct from both the Geneseo and Marcellus black mudstones. In the interest of brevity, the proxy data for these Frasnian units will be presented as a group with attention drawn to similarities and differences among them that are instructive to this study.

The Middlesex Formation (Figs. 4 and 7) is an approximately 5-m-thick interval of interlaminated dark gray and brownish-black noncalcareous mudstone that marks the base of the Sonyea Group and is the first of the Frasnian organic-rich units in western New York (e.g., Rickard, 1975). In general, it is not as organic-rich as the units previously discussed, with average TOC levels of about 3 wt.%. However, there are several thin intervals at the base and top of the unit in which TOC levels rise to 4–6 wt.% (Fig. 7). In western New York, the Middlesex is underlain by the West River Formation—a dominantly medium gray, organic-poor, noncalcareous mudstone containing rare styliolinids and bivalves—and overlain by the Cashaqua Formation—a greenish-gray claystone with some slightly calcareous intervals and abundant pyritized burrow casts. The goniatite and conodont biostratigraphy for this interval is presented in House and Kirchgasser (1993). Middlesex deposition is thought to have occurred during relative sea-level rise (House and Kirchgasser, 1993) and thus represents deeper water deposition than the over- and underlying strata

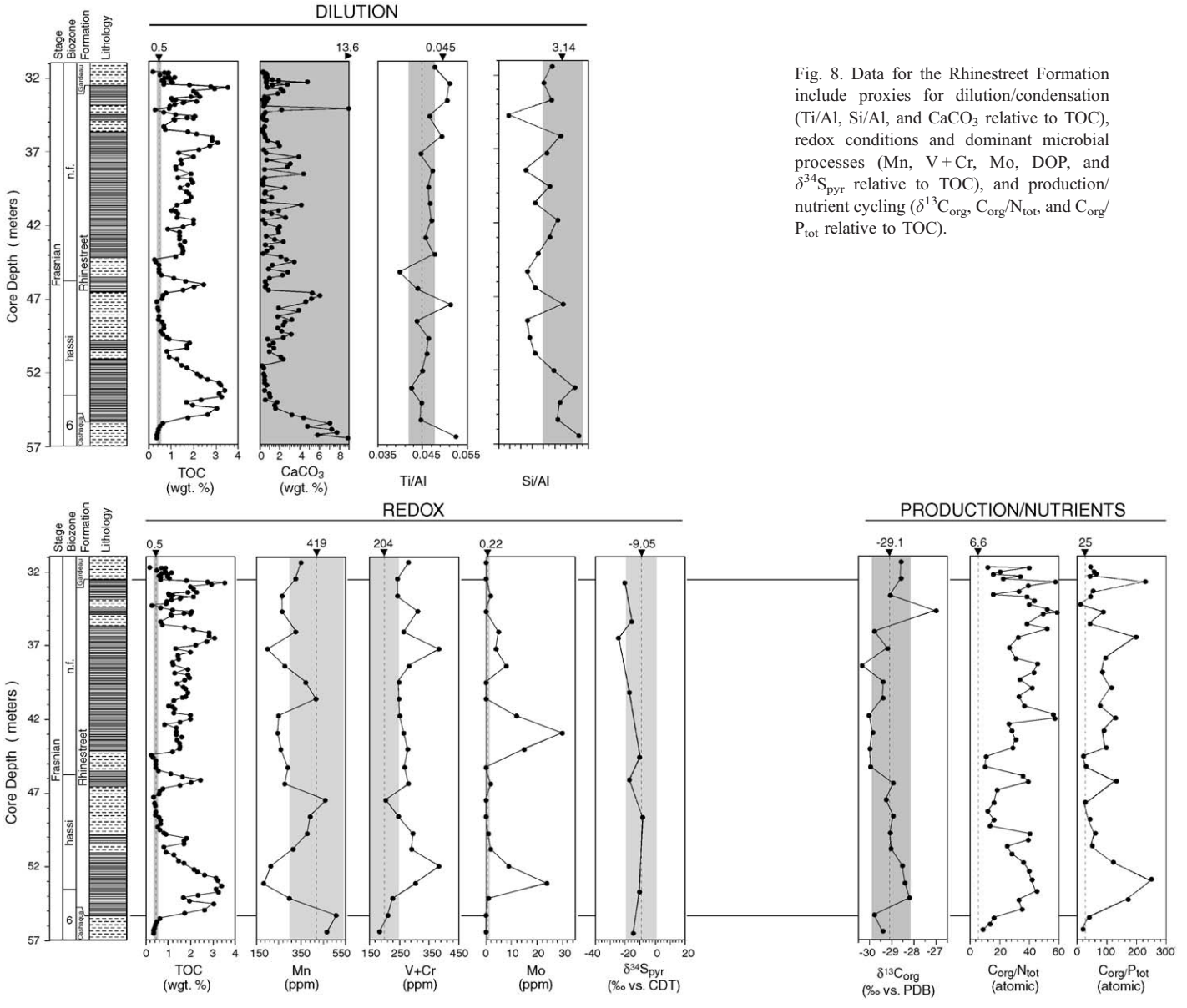

Fig. 8. Data for the Rhinestreet Formation include proxies for dilution/condensation (Ti/Al, Si/Al, and $CaCO_3$ relative to TOC), redox conditions and dominant microbial processes (Mn, V + Cr, Mo, DOP, and $\delta^{34}S_{pyr}$ relative to TOC), and production/nutrient cycling ($\delta^{13}C_{org}$, C_{org}/N_{tot}, and C_{org}/P_{tot} relative to TOC).

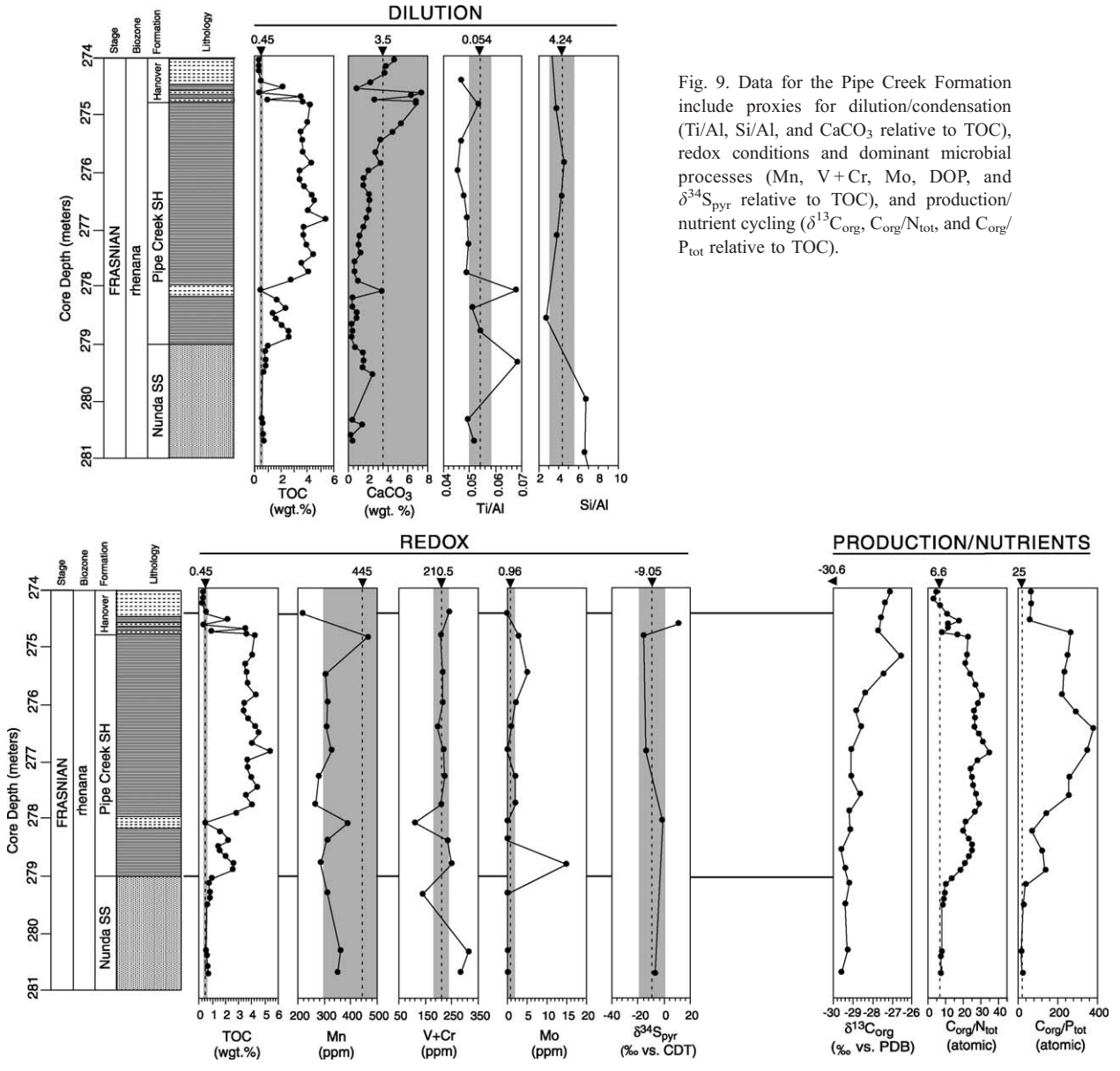

Fig. 9. Data for the Pipe Creek Formation include proxies for dilution/condensation (Ti/Al, Si/Al, and $CaCO_3$ relative to TOC), redox conditions and dominant microbial processes (Mn, V + Cr, Mo, DOP, and $\delta^{34}S_{pyr}$ relative to TOC), and production/nutrient cycling ($\delta^{13}C_{org}$, C_{org}/N_{tot}, and C_{org}/P_{tot} relative to TOC).

of the Cashaqua (Sonyea Group) and West River (Genesee Group) formations.

The Rhinestreet Formation in the study area is a lithologically complex interval, about 25 m thick, including mainly interbedded brownish-black, non-calcareous, laminated mudstone and silty, gray mudstone (Figs. 4 and 8). Organic carbon levels are lower than in any of the units discussed thus far (average 1.8–2.0%; maximum 3.5%), yet they are significantly enriched above 1σ-GSM. The Rhinestreet is the basal formation of the middle Frasnian West Falls Group in western New York (Rickard, 1975) and is underlain by the upper Cashaqua Formation—a slightly calcareous, medium gray to greenish-gray claystone, and overlain by the Gardeau Formation—a silty, medium gray mudstone. In the Akzo core, the Rhinestreet Formation is not formally subdivided as it is in central New York, where four distinct black shale tongues have been defined (the Moreland, Dunn Hill, Roricks Glen, and Corning members; McGhee and Sutton, 1985). It is likely, however, that the four intervals of maximum %TOC identified in the Akzo core (Fig. 8) correspond to these black shale members. The goniatite and conodont biostratigraphy for this interval is presented in House and Kirchgasser (1993). The Rhinestreet Formation is thought to represent deposition during transgression to highstand (House and Kirchgasser, 1993) and thus was deposited in waters deeper than either the underlying Cashaqua Formation (Sonyea Group) or the overlying Gardeau Formation (West Falls Group). However, maximum Rhinestreet sea-level is interpreted to have been lower than that of underlying Middlesex and Geneseo black shales (Ettensohn, 1985a,b). The member-level fluctuations in the Rhinestreet Formation between black shale and gray silty facies were interpreted by Ettensohn (1985b) to represent the interplay of high-frequency sea-level oscillations and cycles of uplift and erosion in the Acadian highlands, which together produced a series of relatively low-duration, alternating episodes of basinal sediment starvation and active progradation of the deltaic complex.

Two additional conspicuous, regionally extensive organic-rich units in the study interval are the Pipe Creek and Dunkirk formations (Figs. 3 and 4). The interval containing these units includes the Frasnian–Famennian stage boundary, as defined by conodont biostratigraphy (Over, 1997). This boundary lies within organic-rich beds of the upper Hanover Formation rather than in the Dunkirk Formation. Based on distinctive positive shifts in the $\delta^{13}C_{org}$ record, Murphy et al. (2000c) established that the Pipe Creek and upper Hanover intervals represent the North American expression of the well-known European Kellwasser events associated with the Frasnian–Famennian (F–F) mass extinction. Thus, detailed sampling was focused on the upper Hanover interval rather than the Dunkirk Formation.

The interval containing the lower Kellwasser Horizon spans, in stratigraphic ascent, the fine-grained sandstone of the uppermost Nunda Formation, the laminated black mudstone of the Pipe Creek Formation, and the silty, greenish-gray mudstone of the lowermost Hanover Formation (Fig. 9). TOC content rises from <1 wt.% in the Nunda to an average of ~ 4 wt.% in the Pipe Creek, and then falls back to <1 wt.% in the Hanover. The upper Kellwasser Horizon spans lithologic transitions between silty greenish-gray mudstone and laminated black mudstone in the upper Hanover Formation (Fig. 10). Concentrations of TOC increase from near-zero to an average of ~ 3 wt.% in the upper Kellwasser black mudstone, dropping back to an average of <1 wt.% above the stage boundary. Goniatite and conodont biostratigraphy for these two units are presented in House and Kirchgasser (1993) and Over (1997).

The overall depositional architecture of the Frasnian through the lowermost Famennian section reflects basinward progradation of the Catskill Delta complex (Fig. 3). The relative deepening events that led to deposition of organic-rich units have been interpreted to result from renewed tectonic activity in the Acadian orogen, resulting in foreland basin subsidence that temporarily interrupted clastic infilling of the basin (tectophase model: Ettensohn, 1985a,b). It has been suggested, however, that only two intervals in the Devonian stratigraphic succession of the Appalachian basin show strong evidence of peripheral bulge uplift (the Wallbridge and Taghanic unconformities) indicating lithospheric flexure related to foreland subsidence (Hamilton-Smith, 1993), and only one of these (the Taghanic) corresponds to a black shale in the study interval. Every major black shale discussed herein does, however,

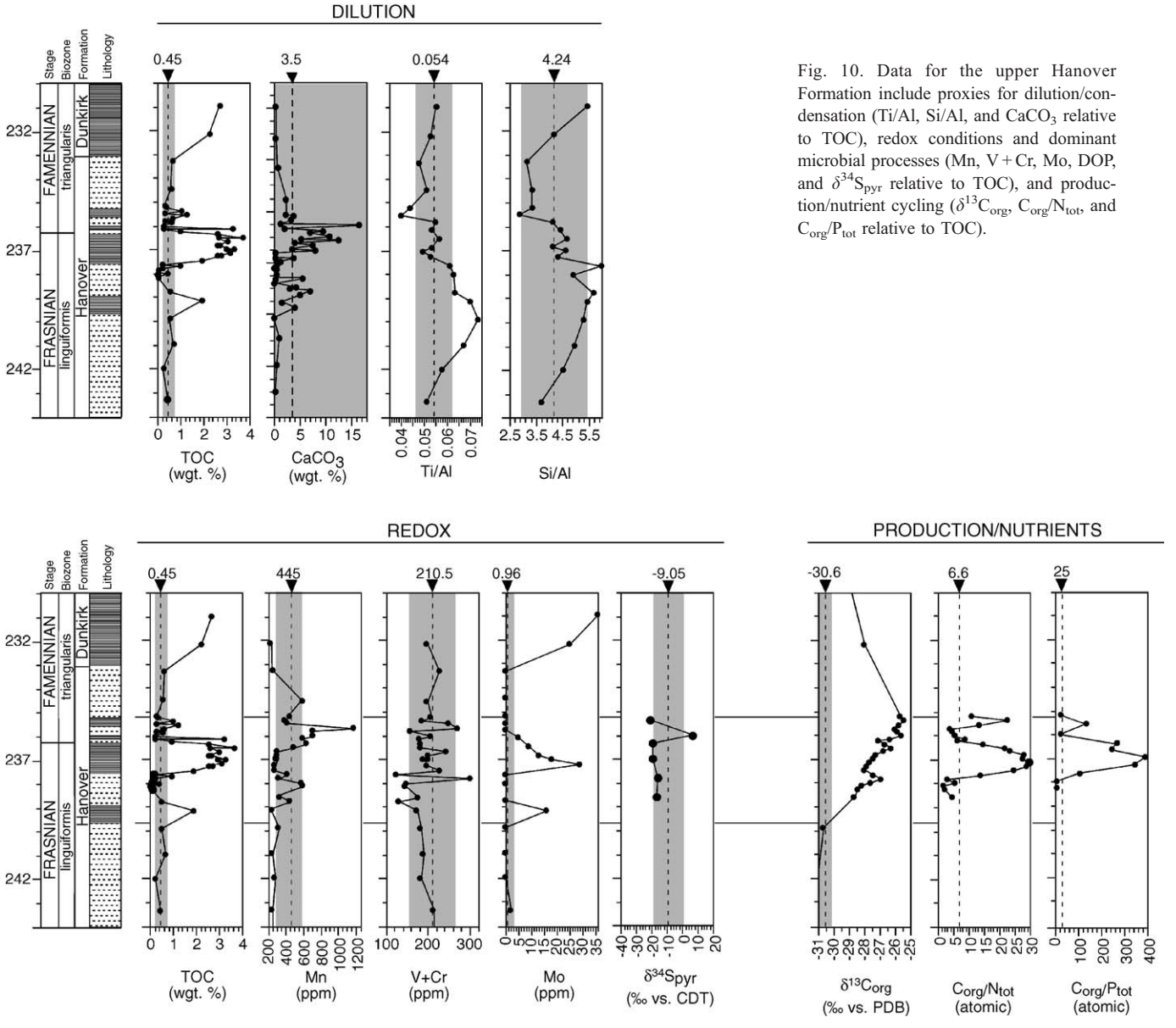

Fig. 10. Data for the upper Hanover Formation include proxies for dilution/condensation (Ti/Al, Si/Al, and $CaCO_3$ relative to TOC), redox conditions and dominant microbial processes (Mn, V + Cr, Mo, DOP, and $\delta^{34}S_{pyr}$ relative to TOC), and production/nutrient cycling ($\delta^{13}C_{org}$, C_{org}/N_{tot}, and C_{org}/P_{tot} relative to TOC).

correspond with a proposed eustatic rise based on study of other sedimentary successions (Johnson and Sandberg, 1988). Subsidence of the foreland basin was clearly essential for accommodation of the basin fill, and although it is impossible to precisely quantify the relative contributions of tectonic and eustatic mechanisms to the rate of change in accommodation during each event of organic-rich deposition, the continuous westward shift of the depocenter during the Frasnian suggests a diminished role for tectonic subsidence during this time.

4.3.1. Dilution/condensation

Several factors suggest increasing dilution in the Frasnian section. Among the geological observations for this are the increased thickness of gray shales (Cashaqua, Angola, Hanover formations), the appearance of silty to sandy facies (e.g., Nunda Formation), and the westward migration of the shoreline (Dennison, 1985). Geochemical data also reflect higher detrital input. With the exception of one concretionary carbonate horizon in the Middlesex Formation, $CaCO_3$ values fall to less than 10% in most Frasnian units, with a GSM of 3.5% in the West Valley core (a 74% decrease from Akzo GSM for $CaCO_3$). Coincidentally, GSM values for Ti/Al and Si/Al increase by 17% and 26%, respectively, between the Akzo and West Valley cores (although the West Valley location is farther west, the progradation of the depositional system would have likely made the two localities quite similar in terms of transport distance from shore). As in the Marcellus and Geneseo formations, the detailed data in Figs. 7–10 show a decrease in Ti/Al to below 1σ-GSM associated with the onset of each organic-rich interval. The pattern is even better illustrated in the 10-point moving average plot (Fig. 4), where clear decreases in Ti/Al precede each black mudstone interval, and increased Ti/Al is associated with subsequent gray mudstone deposition in most cases. These data suggest that relative condensation continues to play a role in the accumulation of OM.

With the exception of the Middlesex Formation, Si/Al ratios display a pattern opposite to the Marcellus and Geneseo formations (Figs. 7–10). In the Middlesex, Si/Al values exceed 1σ-GSM, and this increase (to 4.5, a value similar to Oatka Creek) parallels an increase in TOC content. In the overlying organic-rich units, Si/Al values decrease to GSM or fall below 1σ-GSM in association with organic-rich deposition (Figs. 8–10). This pattern could either reflect decreased sensitivity of the Si/Al proxy under conditions of net increase in detrital flux, a secular decrease in the background eolian Si flux due to a change in climate (cooler? wetter?), or a major change in the contribution of biogenic Si during Frasnian black mudstone deposition.

4.3.2. Decomposition/redox state

Redox-sensitive proxies in Frasnian organic-rich units generally show patterns similar to those of the Geneseo Formation. For example, Mn values consistently fall to levels below 1σ-GSM in association with increased TOC content and increase in adjacent gray mudstones. Evidence for significant oscillation in redox conditions, which might allow for enhanced precipitation of Mn, is suggested by the peak value of almost 1200 ppm immediately overlying the F–F black mudstones in the upper Hanover interval (Fig. 10); the concomitant increase in $CaCO_3$ suggests that Mn was deposited as Mn-carbonate. The V + Cr proxy shows enrichment to levels above 1σ-GSM in association with increased TOC in the Middlesex and Rhinestreet formations. There is no obvious V + Cr trend in the Pipe Creek Formation, but the data in the upper Hanover interval again suggest high frequency oscillations (Fig. 10). Molybdenum is enriched to Geneseo-like levels (15–30 ppm) in samples of the Frasnian black mudstone, but on average, Mo levels are only slightly enriched above 1σ-GSM. Interestingly, maxima in V + Cr appear to lag behind maxima for Mo content by in the Middlesex and Rhinestreet. Lastly, $\delta^{34}S_{pyr}$ values in the Frasnian black mudstone show slight depletion relative to GSM but are generally within 1σ-GSM. Together, these data favor nitrate reduction over sulfate reduction as the dominant anaerobic metabolism, suggesting prevalence of dysoxic conditions during black mudstone deposition.

4.3.3. Production/nutrient cycling

Petrographic analysis of preserved OM in samples from Middlesex, Rhinestreet, Pipe Creek, and upper Hanover black mudstones indicates 95% amorphous kerogen with trace palynomorphs and acritarchs and 5% herbaceous structured material. Samples from

adjacent gray mudstones were generally identical to the black facies, although two samples from Hanover gray mudstones had OM constituents that were 90% amorphous, 5% herbaceous, and 5% woody. Overall, Frasnian mudstones are characterized by continued dominance of marine OM.

Perhaps the most significant differences between the Frasnian organic-rich units and those of the Geneseo and Marcellus are the positive excursions in $\delta^{13}C_{org}$ that characterize events of enhanced OM burial. In the Middlesex Formation, the C-isotope shift is about 1 ‰ This shift is associated with increases in the C_{org}/N_{tot} and C_{org}/P_{tot} ratios up to maximum values of 3 × and 10 × (Redfield) background, respectively. In the Rhinestreet Formation, a positive shift in $\delta^{13}C_{org}$ of over 1 ‰ is followed by a negative shift of about 2 ‰, then another positive shift of at least 3 ‰ (Fig. 8). Organic-rich intervals in the Rhinestreet also show correlative increases in C_{org}/N_{tot} and C_{org}/P_{tot} ratios that reach maximum values of 7–9 × and 6–10 × (Redfield) background, respectively. Comparing these two intervals, the major difference appears to be the trend toward isotopic depletion and a greater increase in C_{org}/N_{tot} in the Rhinestreet Formation.

In association with the lower and upper Kellwasser horizons, there are positive $\delta^{13}C_{org}$ shifts of at least 4 ‰ (Figs. 4, 9, and 10). These events exceed the range of any other isotopic shifts recorded in this study. Associated with each are increases in C_{org}/N_{tot} and C_{org}/P_{tot} ratios. In the Pipe Creek Formation, the maximum values are about 6 × and 15 × (Redfield) background, respectively, and in the upper Hanover Formation, they are about 4.5 × and 16 ×, respectively. Like the Middlesex and Rhinestreet formations, the changes in C_{org}/N_{tot} and C_{org}/P_{tot} ratios track the increases in %TOC quite closely.

4.3.4. Summary

Frasnian organic-rich mudstones differ in several important respects from those of the Marcellus and Geneseo formations. Even though it appears that OM accumulation was initiated by, or associated with, siliciclastic sediment starvation as before, the evidence suggests that detrital flux was generally higher than during deposition of the underlying organic-rich units. This relationship may account for lower average TOC levels in Frasnian black mudstones. Indicators of increased dilution, as well as redox-sensitive proxies that suggest a relatively low frequency and/or duration of anoxic conditions favorable to OM preservation (i.e., Hartnett et al., 1998), suggest that enhanced production may have contributed significantly to the formation of the organic-rich strata. Evidence supporting this conclusion may be found in the positive excursions in $\delta^{13}C_{org}$ that occur in association with Frasnian black mudstone units.

5. Summary and conclusions

Devonian organic-rich deposits have played an influential part in the long history of black shale studies. Throughout this history, the cause of OM burial in the Appalachian foreland basin has been attributed to enhanced preservation under anoxic conditions due to long-term stability of a pycnocline within a relatively deep water column (Pompeckj, 1901; Twenhofel, 1915; Byers, 1977; Ettensohn, 1985a,b; Ettensohn and Barron, 1981; Potter et al., 1982; Brett et al., 1991; Kepferle, 1993). In recent years, however, evidence has accumulated that does not support this interpretation (e.g., Pashin and Ettensohn, 1991; Schieber, 1999; Murphy et al., 2000a,b), suggesting a need to reassess the dominant paradigm. Initially stimulated by the unconventional conclusions of Kauffman (1981) on the Jurassic Posidoneinschiefer, this challenge to the "stagnant basin" model has been repeated in numerous studies of ancient (e.g., Sageman, 1985; Wignall and Hallam, 1991; Oschmann, 1991) and modern (Pedersen and Calvert, 1990) organic-rich sedimentation.

The conventional stagnant basin model has reflected, in part, a lack of detailed information from individual organic-rich units. However, the detailed data presented herein show a systematic range of variations, with three main types of black mudstones identified based on the following characteristics: (1) maximum TOC levels, strong evidence for frequent sulfide in the water column, and no preferential change in $\delta^{13}C_{org}$ (Marcellus); (2) moderate TOC levels, evidence for infrequent sulfide in the water column, and a distinct negative shift in $\delta^{13}C_{org}$ (Geneseo); and (3) low to moderate TOC concentrations, evidence for infrequent sulfide in the water column, and distinct positive shifts in $\delta^{13}C_{org}$ (Mid-

dlesex–Hanover). The succession of changes in these mudstones tracks a long-term trend in basin evolution, the progradation of the Catskill delta, and thus suggests that dilution was a predominant control on OC burial flux.

5.1. Dilution/condensation

The regional geologic data (Fig. 3) indicate that deposition of each black mudstone was associated with shoreline transgression (Rickard, 1975). These data also confirm the progressive basinward progradation resulting from filling of the foreland (Fig. 3). This observation suggests gradual eustatic fall, decaying subsidence of the foreland basin, or a combination of both. Regardless of the cause, relative sea-level shallowed through time as the flux of detrital material to the basin increased (note that the lithofacies baselines in the plot for "Relative Sea-level" in Fig. 4 are slanted, reflecting this long-term trend; in addition, dashed lines that diverge from lithofacies patterns are based on the Ti/Al curve; see discussion below). This conclusion is supported by observed changes in detrital or detrital-influenced elements. For example, average $CaCO_3$ content decreases markedly above the Genesee Group (Fig. 4), whereas average Ti and Si contents increase from the Akzo to the West Valley cores (Table 1; note that the average value for %Al is identical between the two cores). The Ti/Al ratio was employed as a key proxy for detrital input in this study based on the bulk of our observations. However, before the major interpretations are discussed, some explanation of the Ti/Al proxy is needed.

In most pelagic marine sediments, the source of excess Ti is interpreted to be predominantly eolian (Boyle, 1983; Schimmield, 1992; Bertrand et al., 1996). Accordingly, trends of increased Ti/Al (and decreased Si/Al) in organic-rich intervals have been noted in some studies (Caplan and Bustin, 1996; Wortmann et al., 1999). In our study, comparison of petrographic data, Si/Al ratio, and trends in Ti/Al did not support the conclusion of eolian flux as the sole source of Ti-bearing grains in the Appalachian basin. Although it is possible that the Si/Al enrichment may reflect a biogenic source (Schieber et al., 2000), and the absence of a sustained minimum of Ti/Al in the unit most likely to represent maximum condensation (Marcellus) could imply an added source of eolian Ti, for the most part trends in Ti/Al match the regional stratigraphic trends mentioned above. It seems probable, given Schieber's (1999) interpretation that a significant portion of fine-grained transport to the distal basin occurs by gravity flows, that supply of heavier mineral grains derived from fluvial sources would vary in proportion to their abundance and basinward delivery on the adjacent shelf. Thus, increased Ti concentration relative to background Al would reflect relative sea-level fall and progradation and vice versa.

A further window into the controls on Ti supply to the basin is suggested by the apparently anomalous pattern of Ti/Al across the transition from Tectophase II to III (Fig. 4). Ti/Al reaches a minimum value in the Moscow Formation, and then increases across the Taghanic unconformity and through the Genesee Group showing relatively little association to major facies changes (although there is a small decrease at the onset of Geneseo deposition). A possible explanation for this is that the lowest secular Ti/Al values correspond to the last phase of tectonic quiescence, when topographic gradients and terrestrial input were at a minimum. Perhaps the tectonic driver for foreland subsidence that initiated Tectophase III (collision and uplift in the Acadian orogen) actually started during Moscow deposition and began to influence sedimentation in the basin before it influenced subsidence (through elevated topography, enhanced weathering of source rocks, increased gradients, and higher fluxes of Ti to the basin). This effect, however, was later balanced against the rate of increase in accommodation (due to foreland subsidence and eustatic sea-level rise) which first led to clastic cut-off and development of a carbonate platform in the basin depocenter to the east (Tully Limestone). With continued subsidence the platform was drowned, the depocenter migrated westward, and widespread deposition of organic-rich mudstones occurred (Geneseo Formation). The long-term trend in Ti/Al provides supporting evidence that ultimately the flux of siliciclastic material from the newly uplifted orogen overwhelmed the subsidence/eustatic effect and diluted OM leading to gray shale deposition in the Penn Yan Formation (note a similar pattern in the Skaneateles Formation, Fig. 4).

Thus, this shallow, hemipelagic but mud-dominated succession is interpreted to be distinct from the environments sampled by Caplan and Bustin (1996) and Wortmann et al. (1999), and changes in Ti/Al ratio are interpreted to reflect changes in bulk sedimentation, with baseline shifts controlled by changes in long-term basin evolution. The short-term decrease in Ti/Al that accompanies the onset of each black mudstone suggests that condensation was important in the initiation of OM burial (Fig. 4). However, OM burial does not correlate with each decrease in Ti/Al (Fig. 4), indicating that other factors are also necessary for OC accumulation to occur. Note that cases of decrease in Ti/Al without OC enrichment correspond to periods of relative low sea-level in the basin and may reflect higher frequency relative sea-level changes (i.e., subsequences: Brett, 1995).

5.2. Decomposition/redox state

The data for redox-sensitive proxies allow delineation of predominant microbial regimes based on time-averaged accumulation of key reaction products. These data indicate that anoxic–sulfidic conditions were only dominant in the water column during deposition of two relatively thin stratigraphic intervals: the Bakoven member and the unnamed member of the Oatka Creek Formation (Fig. 5). These truly euxinic units accumulated during the maximum deepening of the Appalachian basin within the studied interval (Fig. 4). All other black mudstones showed significantly decreased levels of the proxies indicating sulfate reduction, and are interpreted to have experienced a range a conditions from oxic to suboxic, with relatively infrequent anoxic–sulfidic conditions in the water column. This may suggest a more prominent role for nitrate reduction, especially considering a predominantly oscillating redox system. It also raises the question of enhanced production because, despite the evidence for infrequent sulfide in the water column, TOC levels are nonetheless relatively enriched above GSM. Overall, the redox evidence suggests that water column stratification (e.g., a near permanent halocline) was not a stable feature of the water column. A more likely scenario to account for the redox data is the development of summer thermoclines, which under greenhouse climate conditions may have been only partially mixed for periods of years to 100's of years.

5.3. Production/nutrient cycling

In all of the studied black mudstones, the ratios of C/N and C/P show significant decoupling relative to a Redfield base level. This decoupling covaries closely with the trends in %TOC, suggesting a relationship between decompositional remineralization of OM, release of nutrients, and higher burial fluxes of OC. If such nutrients were recycled to the surface waters, as might occur during seasonal (or longer term) mixing events that broke down thermal stratification, there would be an internal mechanism for enhanced phytoplanktic production, which in light of observed trends in all proxies would provide an explanation for increased burial fluxes of OC. Although this model is internally consistent, and provides a reasonable explanation for many proxy observations, it does not offer a conventional explanation for the carbon isotope data. The potential controls on $\delta^{13}C$ of preserved OM include changes in the isotopic composition of the carbon reservoir supplying autotrophs, changes in the size of the reservoir utilized by autotrophs, changes in the extent of fractionation from that reservoir during photosynthesis due to variations in autotroph growth rate or cell geometry (Bidigare et al., 1997; Popp et al., 1998), or changes in heterotrophy, which confers an additional carbon isotopic fractionation between volatilized waste and refractory waste and biomass (DeNiro and Epstein, 1978). Phytoplankton discriminate in favor of ^{12}C during photosynthesis, and geologically protracted events of enhanced primary production are typically characterized by burial of light carbon, which tends to shift the $CO_{2(aq)}$ reservoir toward ^{13}C, and consequently preserved $\delta^{13}C_{org}$ toward more enriched values (e.g., Scholle and Arthur, 1980).

Higher nutrient availability should have increased phytoplanktonic growth rates, decreased photosynthetic isotope fractionation, and led to ^{13}C-enriched biomass. However, in the Marcellus subgroup, there is no preferred trend, and in the Geneseo the opposite trend is observed. Changes in reservoir size and heterotrophy can be ruled out as dominant causes for observed changes in $\delta^{13}C_{org}$. Although

basin volume may have varied due to changing sea-levels, there is no reason to assume the basin became isolated from the atmosphere, and the rate of change in basin volume must have been considerably less than the air–sea mixing rate for CO_2. As for heterotrophy, although the $\delta^{13}C_{org}$ of bioturbated sediments may be enriched by about 1‰ relative to adjacent laminated sediments (e.g., Pratt, 1984; Murphy et al., 1998), the extent of fractionation and lack of correlation between trends in $\delta^{13}C_{org}$ and bioturbation in the Akzo and West Valley cores argue against this as a dominant mechanism. Changes in carbon sources with different isotopic compositions are suggested for some intervals by the data in Fig. 4. For example, some of the most enriched $\delta^{13}C_{org}$ values are correlated with the maximum secular lowstand when the supply of terrestrially derived OM to the basin would have been highest (Moscow Formation). Conversely, many of the most depleted values in the Hamilton Group correspond to carbonate beds that probably include material derived from the carbonate platform that lay cratonward of the Appalachian foredeep (Brett and Baird, 1996). Note that this trend is observed mainly during the falling sea-level stage of the Hamilton Group, does not apply to post-Geneseo deposits with low carbonate content, and there is no correlation of $CaCO_3$ and $\delta^{13}C_{org}$ within black mudstones. In fact, Murphy et al. (2000b) demonstrated that the depletion in bulk $\delta^{13}C_{org}$ within the Geneseo was attributable to changes in the marine algal contribution to preserved OM.

A possible explanation of short-term changes in the $\delta^{13}C_{org}$ record comes from consideration of the effect of seasonal instability in the water column. Murphy et al. (2000b) argued that the ^{13}C-depleted OM of the Geneseo could reflect a change in the $\delta^{13}C$ of $CO_{2(aq)}$, as would occur if bottom waters rich in isotopically depleted respired CO_2 were mixed to the surface (e.g., Saelen et al., 1998; Rohl et al., 2001). In order for a depleted signal to be preserved, this process would have to have overwhelmed the effects of enhanced nutrient supply and rapid growth. Murphy et al. (2000b) hypothesized that this might occur if productivity during water column mixing events was N-limited. There are two pieces of evidence that provide support for this possibility: (1) while there is at least a 10-fold increase in P-release from OM relative to C associated with maximum OC burial, there is only ~3–4-fold increase in N-release (Fig. 6); and (2) it is likely that the bottom water nitrate reservoir would have been at least somewhat depleted by denitrification between mixing events. This latter contention is based on data from the modern oceanic oxygen minimum zone, where NO_3^{2-}/PO_4^{3-} ratios may be significantly less than the typical ~16:1 as a consequence of denitrification (Tyrrell and Law, 1997). Denitrification is a more efficient metabolic pathway for bacteria than is sulfate reduction (Stumm and Morgan, 1981), so if nitrate is abundant in oxygen-depleted bottom waters, denitrification may be the dominant anaerobic metabolism. If this were the case during Geneseo deposition, it would explain the lack of evidence for persistently or pervasively sulfidic conditions in bottom waters, as bacterial sulfate reduction may have been a process of secondary importance relative to nitrate reduction and denitrification.

Thus, it may be that NO_3^{2-} availability limited productivity immediately following water column mixing, leaving unused PO_4^{3-} and isotopically depleted $CO_{2(aq)}$ in surface waters to be utilized over time as N-fixation made more nitrate available. This would likely cause a more protracted duration of elevated productivity than is typical of algal blooms, and a lower rate of productivity than might be expected to result from rapid nutrient infusion, allowing the isotopic composition of upwelled $CO_{2(aq)}$ to exert the dominant control on the $\delta^{13}C$ of carbon being fixed as biomass. OM flux to the sediment would be sufficiently high, however, to keep the entire sediment column anoxic despite the frequent presence of O_2 in bottom waters. In the units overlying the Geneseo Formation, this same process may have occurred, but a critical threshold was reached after which the influence of increased production on C-isotope fractionation dominated over the influence of upwelled $CO_{2(aq)}$ (e.g., Middelburg et al., 1991). In the case of the Rhinestreet Formation, oscillation of $\delta^{13}C_{org}$ from relatively enriched to depleted suggests shifting dominance between the two modes. There is a final factor to consider in explaining the Frasnian isotopic record. If Frasnian sea-level rise events were eustatic, and the process accounting for OM burial in the Appalachian basin was repeated at

all latitudes with seasonal variability, then the enriched $\delta^{13}C_{org}$ values in these black mudstones might also reflect shifts in the global carbon reservoir related to net OM burial. Global carbon burial, for whatever cause, is the preferred interpretation of the intercontinentally expressed $\delta^{13}C_{org}$ shifts at the two Kellwasser horizons (e.g., McGhee, 1996; Joachimski, 1997).

Remineralization of OM and increased nutrient recycling have been discussed as a possible explanation for organic-rich deposits ranging from Paleozoic to Pleistocene age (Middelburg et al., 1991; Ingall et al., 1993; Calvert et al., 1996; Caplan and Bustin, 1996, 1999). The Devonian is a somewhat unique period, however, because the diversification and spread of vascular plants during this time is believed to have resulted in a significant increase in aluminosilicate weathering rates and thus greater fluxes of nutrients to the world's oceans (Berner, 1997). As a result, increased flux of terrestrially derived nutrients has been proposed to account for increases in Late Devonian productivity and consequent OC burial events (Algeo et al., 1995; Joachimski et al., 2001). Although it is likely that the global inventory of primary production did increase during this time, there are several problems with the terrestrial nutrient hypothesis as a proximate explanation for the narrow stratigraphic intervals of OC-enriched mudstones in the distal Appalachian basin. Fluvial nutrient delivery is typically confined to near-estuarine environments, except at the mouths of continental-scale watersheds like the Amazon River (Van Der Zwann and Jorissen, 1991). Watersheds of this scale seem unlikely given the geographic proximity of the Acadian orogen and the Appalachian foreland basin, as well as the interpreted paleolatitude and prevailing climate. It is difficult to envision why, in the early stages of the spread of vascular plants, riverine nutrient flux to distal basin sites would have increased during short intervals, and especially those characterized by rising sea-levels. Coastal nutrient confinement should have been enhanced by the marine transgressions associated with black mudstone deposition, when a higher proportion of the riverine nutrient load was fixed by increased production in expanded estuaries. Finally, in the data compilation of Retallack (1997), several indicators of large vascular plant development for which there are data points through our study interval (e.g., maximum thickness of fossils stems and trunks, coal seam thickness, total floral diversity) do not show major increases until mid- to Late Frasnian time or thereafter. Although the evolution of vascular land plants was surely underway by the Late Eifelian, and a trend of increase in silicate weathering, nutrient release, net global primary production, and concomitant CO_2 drawdown had probably begun (Berner, 1997), this set of processes is unlikely to have provided the proximate mechanism for OC-rich mudstone deposition in the Appalachian basin.

5.4. A synthetic depositional model

The depositional model that we propose as the best explanation for the origin of the studied organic-rich mudstones has three master controlling variables:

Seasonal thermoclines: Evidence for wave base impingement in distal fine-grained facies (e.g., Schieber, 1999), for benthic colonization events by opportunistic species (e.g., Thompson and Newton, 1987; Brett and Baird, 1997), and lack of evidence for long-term anoxic–sulfidic conditions in the black mudstones (except Marcellus) are consistent with the conclusions of Tyson and Pearson (1991) that seasonal dysoxia–anoxia related to thermal stratification is a more actualistic model for the behavior of ancient epeiric seas at shelfal depths. Climatic cooling on the background of a Paleozoic greenhouse, which has been suggested for the Eifelian–Famennian interval (Scotese and McKerrow, 1990; Copper, 1986; Buggisch, 1991; Isaacson et al., 1997) and is consistent with the observations of Berner (1997) concerning pCO_2 trends, would have enhanced seasonality, and thus progressively increased the stratification-mixing effect during the study interval.

Nutrient supply: The data indicating predominance of algal OM in mudstone facies suggests that use of the Redfield ratio as a C/N/P baseline is reasonable. Marked decoupling of C/N/P is observed in every black mudstone in this study, suggesting

release of a potential reservoir of the bio-limiting nutrients N and P, which under the conditions described above could have periodically upwelled to drive excess new production. In addition, this instability would provide a mechanism for preventing the scavenging of PO_4^{3-} by Fe-oxyhydroxides that occurs at stable chemoclines (e.g., McManus et al., 1997). If the global nutrient inventory was already somewhat higher due to increased terrestrial supply (Algeo et al., 1995), perhaps in situ recycling was just sufficient to drive additional production over the threshold to produce bottom water anoxia (Nijenhuis et al., 2001), although Martin (1996) indicated that most of the Devonian was characterized by oligotrophic conditions. Interestingly, the change to dominance of eutrophic conditions noted by Martin (1996) coincides with the shift to positive isotopic excursions in the Frasnian black mudstones described herein. If seasonality increased during the study interval, as suggested above, then nutrient release may also have increased, thus accounting for the increase in productivity through time. Alternatively, this is the interval in which Retallack (1997) showed the greatest changes in the terrestrial flora, suggesting increased terrigenous nutrient flux.

Relative sea-level: The master proximate variable that initiated, as well as regulated the nature and extent of excess OM burial was relative sea-level change. A combination of tectonic subsidence and eustasy controlled changes in accommodation space, which determined the depth of the water column, the volume of bottom and surface waters, and thus the relative effectiveness of seasonal (or longer term) mixing events and concentrations of microbial reaction products like respired CO_2, nitrate, and phosphate (Fig. 2). When water depth was at a maximum during Marcellus deposition, seasonal mixing rarely penetrated the bottom waters and euxinic conditions prevailed. With the secular decrease in relative sea-level through time (Fig. 4), the effectiveness of annual mixing increased and the "productivity–anoxia feedback" mechanism (Ingall et al., 1993) became a key factor in maintaining high burial fluxes of OC. During this secular decrease in relative sea-level, short-term sea-level rise events were the catalysts for OM burial as they caused sediment starvation and OC concentration in surface sediments. This led to bottom water O_2 depletion, progression to nitrate and/or sulfate-reducing conditions, and enhanced OM remineralization (Fig. 2), which under conditions of oscillating seasonal dysoxia–anoxia primed the eutrophication pump. Cessation of this process was forced by dilution, as the increasing flux of siliciclastics associated with short-term relative sea-level fall progressively lowered surface sediment OC concentrations until demand for O_2 was met by new supply from seasonal mixing.

The study of OM burial in depositional systems of the deep past has advanced rapidly in recent decades, and our current understanding of processes (Figs. 1 and 2) provides an excellent framework within which to approach the problem. However, our inability thus far to precisely constrain time within many organic-rich intervals under study makes it impossible to determine accurate accumulation rates, which would help address some of the most critical unknowns. We are left to analyze relative trends, which in the context of multi-proxy data sets composed of well-chosen independent and dependent parameters provides a reasonable basis for the development of interpretations. As always, however, the limiting factor in these interpretations is the relative strength or "uniformitarian confidence" of the assumptions that must be made in the process. In this study, some of the assumptions that are currently most difficult to test, and need the most attention in the future, concern: (1) Devonian primary producers and bacterial communities, their C/N/P and $\delta^{13}C$ characteristics, and their relative contributions to preserved OM; (2) sources and relative contributions of bio-limiting nutrients; and (3) spatial consistency of trends in geochemical parameters.

The data set discussed herein is representative of a single region where a set of specific environmental conditions determined the relative sensitivity of geochemical proxies. While some of these proxies (Mo, $\delta^{13}C$) are likely to vary consistently as proximity to the Appalachian foreland decreases, others (Ti/Al) may not. Further work on OM burial during the late Devonian must extend the sampling of organic-rich units to the margins of the Appalachian basin and beyond, and

it is hoped that the data presented herein will provide a useful framework for spatial comparisons.

Acknowledgements

This study was supported with funds from the National Science Foundation (EAR-9725441), as well as a Northwestern University Research Grant. The project was conducted in collaboration with a paleobiologic study by Dr. Carlton Brett (University of Cincinnati) and we thank him for both logistical support and helpful discussions. We wish to acknowledge the analytical efforts of XRAL for ICP-MS data, Mike Darnell of the Houston Advanced Research Center for organic petrography, and staff at the Biogeochemistry Lab of Indiana University for sulfur isotopic analyses. The Akzo Nobel Salt Co. and the State Geological Survey of New York were instrumental in providing needed core material. Finally, thanks also go to Juergen Schieber and an anonymous reviewer for helpful reviews of the manuscript. **[EO]**

Appendix A

Table A1
Data tabulation for Marcellus subgroup study interval

Depth (m)	OC (wt.%)	$CaCO_3$ (wt.%)	Al (wt.%)	Ti (wt.%)	Si (wt.%)	V (ppm)	Cr (ppm)	Mn (ppm)	Mo (ppm)	Fe-hcl (wt.%)	Fe-pyr (wt.%)	DOP	N_{tot} (wt.%)	P_{tot} (wt.%)	$\delta^{13}C_{org}$ (‰ vs. PDB)	$\delta^{13}S_{pyr}$ (‰ vs. CDT)
328.17	9.81	2.21	8.03	0.31	21.3	166	77	226	28	1.18	2.03	0.63		0.027	− 29.48	
328.36	3.24	8.50	8.85	0.31	23	195	98	200	47	1.14	1.86	0.62		0.024	− 30.39	
328.57	5.84	1.45	8.17	0.32	22.2	225	103	169	79	1.48	4.81	0.77		0.021	− 30.01	
328.72	4.27	10.85													− 29.46	
328.92	2.71	14.93	8.39	0.33	22.1	155	149	235	5	1.44	0.58	0.29		0.016		− 23.74
329.14	2.72	18.80													− 30.82	
329.28	5.24	0.00													− 30.12	
329.48	0.8	52.31	3.43	0.14	10.5	55	13	417	2	0.91	1.00	0.52		0.015	− 30.33	− 32.9
329.68	0.49	74.70	0.76	0.04	2.46	12	3	523	1	0.26	0.24	0.48		0.023		
329.89	2.17	42.70	3.49	0.15	10.8	57	37	437	2	0.87	0.78	0.47	0.21	0.022	− 30.86	
330	2.04	33.24													− 29.22	
330.1	4.11	8.64	8.44	0.29	24.8	148	91	208	18							
330.2	1.42	51.69													− 30.31	
330.37	4.56	4.63	9.39	0.29	25.4	172	55	212	31	1.06	2.31	0.69		0.018	− 29.76	
330.46	6.09	1.38													− 29.62	
330.53	4.62	0.83											0.27		− 29.50	
330.62	5.83	0.41													− 29.98	
330.73	3.74	0.76													− 29.62	
330.94	5.19	0.76	8.8	0.3	26.2	196	98	147	68	0.93	3.35	0.78		0.017	− 29.65	− 28.93
331.14	5.84	2.83													− 29.40	
331.34	4.53	4.56														
331.6	5.12	1.59													− 30.20	
331.71	6.81	0.00													− 29.63	
331.8	5.21	0.14											0.27		− 30.05	
332.05	8.21	0.76	7.84	0.35	25.5	252	75	161	169	0.93	4.46	0.83		0.026	− 29.72	
332.15	3.68	3.25	8.74	0.3	26.6	183	98	189	27	0.89	1.65	0.65		0.018	− 29.44	
332.26	8.31	0.00													− 29.58	
332.46	10.14	1.45													− 29.97	
332.72	8.61	0.97	7.89	0.32	26.9	331	86	140	236	0.79	4.79	0.86	0.47	0.025	− 29.99	− 32.89
332.92	8.25	1.17													− 29.87	
333.12	8.68	0.00	7.61	0.32	26.4	277	85	146	173	0.67	4.55	0.87		0.033	− 29.69	− 33.56
333.38																

Table A1 (*continued*)

Depth (m)	OC (wt.%)	$CaCO_3$ (wt.%)	Al (wt.%)	Ti (wt.%)	Si (wt.%)	V (ppm)	Cr (ppm)	Mn (ppm)	Mo (ppm)	Fe-hcl (wt.%)	Fe-pyr (wt.%)	DOP	N_{tot} (wt.%)	P_{tot} (wt.%)	$\delta^{13}C_{org}$ (‰ vs. PDB)	$\delta^{13}S_{pyr}$ (‰ vs. CDT)
333.59	14.18	1.59	6.15	0.26	21.7	382	65	129	279	0.42	5.93	0.93	0.67	0.035	− 29.50	
333.85	6.68	1.87	7.79	0.28	26.4	275	87	135	93	0.61	5.04	0.89		0.038	− 29.62	
334.06	7.25	0.00													− 29.77	
334.24																
334.43	9.01	0.00											0.42		− 29.85	
334.63	11.19	1.11	6.29	0.27	23.1	328	54	120	251	0.36	7.56	0.95		0.027	− 29.43	
334.86	11.25	4.22													− 29.79	
335.05	12.84	0.00													− 29.74	
335.26	9.86	0.90	6.09	0.28	24.4	337	71	147	206		5.15	1.00			− 29.76	
335.46	11.71	0.00													− 30.15	
335.67	12.01	0.35													− 29.37	
335.87	9.51	0.00	6.32	0.29	26.1	310	53	154	192	0.50	5.41	0.92	0.38	0.035	− 29.58	− 28.21
336.06	9.87	0.00														
336.27	11.17	0.00	6.02	0.27	23.6	363	71	135	234	0.35	5.05	0.94		0.033	− 29.59	
336.48	9.99	0.00											0.39		− 29.89	
336.69	17.3	0.97	6.48	0.26	20.6	421	58	129	394	0.58	6.35	0.92	0.74	0.03	− 29.74	
336.89																
337.09	11.7	0.00	6.5	0.29	23.4	383	65	125	229	0.51	6.22	0.92	0.42	0.029	− 29.41	
337.2	8.4	0.00	6.34	0.19	17.2	210	44	178	53	0.31			0.32		− 29.71	
337.3	2.19	15.06	9.11	0.33	26	204	60	154	24	0.50	1.58	0.76		0.029		− 9.9
337.41	5.87	0.41	7.82	0.32	23.6	150	68	185	16						− 30.75	
337.5	7.18	0.35	7.47	0.29	21.9	172	85	199	20	0.51	1.56	0.75	0.30	0.029	− 29.74	− 7.76
337.6	6.65	18.31													− 29.57	
337.72	9.74	6.77													− 29.53	
337.83	4.89	34.00	5.21	0.2	14.9	192	59	252	56	0.57	1.62	0.74	0.51	0.019	− 30.29	
337.93	3.96	26.53													− 30.08	
338.13	7.23	1.52													− 29.70	
338.31	7.2	0.00	7.11	0.32	21.8	158	83	216	14	0.67	1.30	0.66		0.013		
338.53	4.81	4.28	8.54	0.38	24.1	150	85	186	15	0.68	1.80	0.73	0.36	0.03	− 30.17	
338.73	7.95	1.04	8.67	0.34	24.4	265	101	165	60	0.51	2.28	0.82		0.026	− 29.74	
338.92	0.81	30.20	6.46	0.24	17.1	95	58	262	3	0.47	1.87	0.80			− 29.58	
339.11	1.19	20.45	7.37	0.29	20.6	108	50	211	3	0.54	1.95	0.78		0.008	− 30.45	− 14.06
339.31	0.39	75.94									1.85	1.00		0.016		
339.51	6.12	5.11											0.47		− 30.14	
339.71	3.77	8.15	8.47	0.33	22.3	280	77	140	51	0.50	2.55	0.84		0.005		
339.89	2.48	34.20														
340.09	1.04	62.26	2.08	0.08	6.45	52	5	216	11	0.30	0.67	0.69		0.015	− 30.23	
340.31	6.86	0.00													− 29.84	
340.5	1.95	24.05	6.99	0.3	18	129	80	194	6	0.49	1.38	0.74		0.029	− 29.17	
340.71	2.42	7.67													− 29.13	
340.87	2.75	10.99	8.7	0.38	21.7	198	91	189	6	0.47	1.85	0.80		0.032	− 30.20	− 1.9
341.09	0.39	75.18	0.23	0.02	0.75	4	0	173	1	0.11	1.72	0.94		0.305	− 31.90	13.41
341.24	0.26	76.84	0.26	0.02	0.71	11	4	265	2	0.21	1.09	0.84		0.299		− 6.66
341.26	0	89.16				109	11		0			0.49	0.06		− 31.19	− 13.94
341.31	2.21	83.83	0.65	0.03	3.76	157	30	177	46			0.67	0.31		− 30.58	
341.36	10.13	45.41	2.63	0.14	10.9	617	66	126	202						− 30.37	
341.41	13.44	40.92										0.78	0.69		− 30.36	− 25.93
341.46	3.37	85.75	0.52	0.02	2.4	186	30	184	61						− 30.42	
341.51	8.35	61.58										0.73	0.66		− 30.49	
341.56	14.74	34.75	3.04	0.14	10.8	743	70	122	298						− 30.57	
341.61	18.08	20.92										0.81	0.66		− 30.73	− 24.35

(continued on next page)

Table A1 (*continued*)

Depth (m)	OC (wt.%)	$CaCO_3$ (wt.%)	Al (wt.%)	Ti (wt.%)	Si (wt.%)	V (ppm)	Cr (ppm)	Mn (ppm)	Mo (ppm)	Fe-hcl (wt.%)	Fe-pyr (wt.%)	DOP	N_{tot} (wt.%)	P_{tot} (wt.%)	$\delta^{13}C_{org}$ (‰ vs. PDB)	$\delta^{13}S_{pyr}$ (‰ vs. CDT)
341.66	13.02	42.66	2.55	0.12	9.45	786	66	99	213						− 30.65	
341.71	17.25	13.67													− 30.26	
341.76	2.25	51.66	4.74	0.18	9.93	250	40	111	9			0.52	0.12		− 30.20	
341.81	0.12	93.16										0.29	0.02		− 29.94	− 17.96
341.86	0	95.50	0.17	0	1.02	6	2	176	0						− 30.01	

Table A2
Data tabulation for Geneseo Formation study interval

Depth (m)	OC (wt.%)	$CaCO_3$ (wt.%)	Al (wt.%)	Ti (wt.%)	Si (wt.%)	V (ppm)	Cr (ppm)	Mn (ppm)	Mo (ppm)	Fe-hcl (wt.%)	Fe-pyr (wt.%)	DOP	N_{tot} (wt.%)	P_{tot} (wt.%)	$\delta^{13}C_{org}$ (‰ vs. PDB)	$\delta^{34}S_{pyr}$ (‰ vs. CDT)
160.16	0.79	4.25													− 28.75	
160.36	0.83	7.58	7.49	0.42	25.4	129	82	338	0	1.66	0.54	0.25	0.081	0.0488	− 28.01	
160.55	0.88	9.00													− 27.85	
160.74	0.88	8.25	8.01	0.43	25.5	133	86	325	0	0.923	0.557	0.38	0.087	0.0425	− 28.09	
160.95	0.75	8.58													− 28.28	
161.14	0.64	7.67											0.075		− 27.94	
161.34	0.83	7.83	8.94	0.46	25.8	145	72	345	0	1.48	0.645	0.3		0.0346	− 27.79	
161.37																− 15.04
161.54	0.89	6.08											0.089		− 29.10	
161.74	0.65	6.58													− 29.18	
161.94	0.58	6.33	7.1	0.33	19.4	115	51	592	1	1.88	0.624	0.25	0.067	0.0397	− 28.50	
162.14	0.74	4.25													− 29.08	
162.31	0.91	2.67											0.090		− 29.42	
162.51	1.02	2.50													− 29.19	
162.72	1.84	2.08	9.12	0.4	24.1	183	99	341	15	1.76	1.15	0.39	0.141	0.0676	− 29.51	
162.91	0.83	37.75													− 29.66	
163.12	1.05	29.33	8.13	0.37	24.7	258	98	273	33	1.66	0.429	0.21	0.097		− 30.14	
163.31	3.96	8.50	8.04	0.37	24.3	312	46	302	23	1.5	0.574	0.28		0.0573	− 30.44	
163.52	1.23	20.33											0.095		− 30.14	
163.74	0.91	31.58													− 30.06	
163.96	2.38	10.08											0.129		− 29.79	
164.15	4.47	8.50	4.95	0.22	14.3	100	55	671	7	1.1	1.06	0.49		0.0655	− 29.89	
164.36	3.61	16.33											0.154		− 30.11	− 9.75
164.48																− 14.5
164.51	3.83	17.25													− 30.16	
164.7	5.79	4.33	6.76	0.3	21.9	133	55	372	6	1.35	0.976	0.42	0.262	0.0908	− 30.16	
164.89	4.89	34.08													− 28.80	
165.08	4.67	9.83											0.252		− 30.36	
165.34	4.79	1.25													− 30.06	
165.53	5.79	1.58											0.186		− 30.13	
165.74	5.59	8.42	7.18	0.3	24	179	78	356	16	1.35	1.17	0.46		0.0909	− 30.17	
165.95	4.69	12.08											0.153		− 30.18	
166.14	6.11	13.92													− 30.02	− 14.6
166.33	4.13	38.00	6.81	0.26	25.5	169	45	336	9	0.745	0.554	0.43	0.194		− 29.55	
166.53	1.25	62.58													− 29.94	
166.73	1.93	31.33											0.126		− 29.61	
166.9	2.83	21.50	6.29	0.27	24.3	269	47	303	28	1.21	0.487	0.29			− 30.09	
167.1	6.4	13.92											0.388		− 29.98	
167.31	1.96	37.92													− 29.80	

Table A2 (*continued*)

Depth (m)	OC (wt.%)	$CaCO_3$ (wt.%)	Al (wt.%)	Ti (wt.%)	Si (wt.%)	V (ppm)	Cr (ppm)	Mn (ppm)	Mo (ppm)	Fe-hcl (wt.%)	Fe-pyr (wt.%)	DOP	N_{tot} (wt.%)	P_{tot} (wt.%)	$\delta^{13}C_{org}$ (‰ vs. PDB)	$\delta^{34}S_{pyr}$ (‰ vs. CDT)
167.53	1.87	31.83	6.45	0.23	24.7	212	84	349	18	1.14	0.45	0.28	0.116	0.0664	− 29.92	
167.73	2.87	21.17													− 29.99	
167.92	3.52	15.42											0.162		− 29.77	
168.1	3.72	12.67													− 29.97	
168.24	3.1	15.00	5.73	0.24	22	154	67	465	22	1.42	0.695	0.33	0.163	0.0713	− 30.21	
168.38	3.31	15.67													− 30.30	
168.55	2.16	12.33											0.137		− 29.88	
168.61	2.61	13.92	7.79	0.34	23.6	155	86	448	7	1.11	0.611	0.35		0.0647	− 30.04	
168.8	3	12.92											0.183		− 30.11	
169.02	4.82	11.00	8.63	0.36	23.6	163	92	430	3	1.32	1.09	0.45		0.0888	− 29.26	
169.21	4.1	15.00											0.148		− 30.05	
169.42	4.12	13.33													− 30.10	
169.62	4.84	9.08	8.54	0.32	26	166	96	254	4	0.871	0.603	0.41	0.148	0.0737	− 29.93	
169.83	4.6	8.58													− 29.75	
170.03	5.11	8.67											0.165		− 29.83	
170.24	4.49	14.33	8.37	0.32	25.8	150	92	320	2	1.14	0.834	0.42		0.0870	− 29.60	
170.45	4.31	18.67											0.199		− 29.51	
170.65	2.94	17.08													− 29.48	
170.76	4.26	16.00	8.33	0.32	24.1	155	88	436	0	1.23	0.821	0.4	0.185	0.1169	− 29.41	
170.97	2.84	24.42													− 29.20	
171.17	2.1	14.17											0.138		− 29.28	
171.36	2.53	16.17													− 29.26	
171.46	1.67	11.25	8.42	0.4	24.1	156	100	360	0	1.89	0.733	0.28	0.127	0.1442	− 29.41	
171.57	1.39	0.17													− 29.41	5.5
171.78	1.18	4.25											0.113		− 29.40	
171.98	1.1	5.67													− 29.52	
172.16	0.48	9.00	8.97	0.38	25.1	167	56	348	0	1.75	1.83	0.51	0.062	0.0949	− 28.92	
172.37	0.47	6.58													− 28.91	5.53
172.58	0.53	5.42											0.071		− 30.91	
172.77	0.54	5.58	8.88	0.4	25.9	161	99	300	0	2.28	0.772	0.25		0.0939	− 31.50	
172.97	0.36	4.25											0.051		− 27.94	
173.17	0.35	3.42													− 28.18	
173.37	0.36	3.42	8.96	0.32	25	167	84	281	0	2.07	1.49	0.42	0.051		− 28.09	
173.55																12.01
173.57	0.37	3.67													− 27.61	
173.64	0.35	2.75	9.34	0.41	26.3	170	105	267	1				0.053		− 27.73	
173.84	0.31	2.67	9.49	0.37	25.7	177	58	263	0	2.39	0.341	0.12		0.0938	− 27.51	
174.03	0.32	2.50											0.041		− 27.58	
174.45	0.45	8.64	8.42	0.39	23.7	150	93	406	0						− 27.65	

Table A3
Data tabulation for Middlesex Formation study interval

Depth (m)	OC (wt.%)	$CaCO_3$ (wt.%)	N_{tot} (wt.%)	P_{tot} (wt.%)	$\delta^{34}S_{pyr}$ (‰ vs. CDT)
114.57	1.09	1.25	0.14		
114.65	0.3	1.00	0.04		
114.72	0.47	1.17	0.08		
114.9	0.52	0.00	0.10	0.047	− 9.39
114.97	0.79	0.17	0.14		
115	0.41	0.67	0.08		
115.04	0.85	1.25	0.16		

(continued on next page)

Table A3 (*continued*)

Depth (m)	OC (wt.%)	$CaCO_3$ (wt.%)	N_{tot} (wt.%)	P_{tot} (wt.%)	$\delta^{34}S_{pyr}$ (‰ vs. CDT)
115.11	0.51	0.00	0.11		
115.19	0.95	1.50	0.17		
115.23	0.11	0.92	0.02		
115.28	0.49	1.08	0.04		
115.31	1.18	1.17	0.07	0.046	
115.34	0.56	0.00	0.02		
115.37	1.04	0.83	0.05		
115.4	0.59	0.00	0.03		
115.42	0.97	0.08	0.08		
115.48	0.67	0.92	0.04		
115.54	2.52	0.25	0.14		
115.62	3.99	1.25	0.17		− 15.42
115.71	3.61	1.17	0.20	0.041	
115.81	2.68	1.25	0.12		
115.91	1.8	0.75	0.11		
116.08	0.43	0.58	0.07	0.050	
116.16	0.74	1.17	0.15		
116.22	0.53	0.08	0.10		
116.26	0.62	1.17	0.12		
116.31	0.31	0.00	0.06	0.049	
116.36	0.39	0.75	0.06		
116.4	0.69	0.33	0.10		− 6.99
116.47	0.33	1.33	0.05		
116.53	0.73	0.17	0.13	0.055	
116.62	0.65	1.08	0.12		
116.77	1.55	1.33	0.30		
116.92	2.12	0.00	0.34	0.063	
117.22	3.23	0.00	0.22		
117.37	2.59	0.17	0.13		
117.57	2.16	0.58	0.12	0.040	
117.72	1.11	0.67	0.06		
117.87	1.58	1.08	0.12		
118.02	1.7	0.83	0.12		− 18.56
118.18	1.76	0.58	0.13	0.046	
118.46	2.65	0.67	0.16		
118.61	2.31	0.00	0.11		
118.8	2.6	0.75	0.16	0.039	
118.95	2.8	1.00	0.19		
119.1	3.19	0.00	0.26		
119.26	2.64	0.00	0.17		
119.4	3.29	0.83	0.19	0.037	− 17.93
119.7	2.55	0.08	0.18		
119.86	2.68	0.00	0.14		
120.02	3.42	0.58	0.18	0.041	
120.17	2.75	0.00	0.12		
120.32	3.45	0.58	0.19		
120.47	3.23	1.17	0.15		
120.63	3.25	3.50	0.19	0.044	
120.93	3.09	5.08	0.16		
121.08	1.91	77.41	0.09		
121.2	5.25	5.83	0.26	0.044	
121.35	5.93	2.17	0.21		− 13.81
121.5	2.64	0.75	0.14		
121.78	0.73	2.50	0.07	0.053	

Table A3 (*continued*)

Depth (m)	OC (wt.%)	$CaCO_3$ (wt.%)	N_{tot} (wt.%)	P_{tot} (wt.%)	$\delta^{34}S_{pyr}$ (‰ vs. CDT)
121.91	0.55	3.33	0.06		
122.23	0.44	3.50	0.06		
122.34	0.66	2.25	0.10	0.050	
122.49	0.69	3.17	0.10		
122.64	0.48	3.67	0.08		
122.79	0.48	2.75	0.07		
122.94	0.6	3.58	0.08	0.053	
123.24	0.65	2.50	0.12		
123.4	1.13	4.67	0.19		
123.56	0.68	3.17	0.12	0.048	
123.71	1.01	3.92	0.10		
123.86	1.49	5.08	0.14		− 17.87
123.95	0.92	6.00	0.09		
124.09	0.19	4.17	0.04	0.043	
124.24	0.25	4.08	0.05		
124.39	0.37	3.08	0.07		− 17.03
124.54	0.32	7.33			
127.49					− 17.34

Depth (m)	OC (wt.%)	$CaCO_3$ (wt.%)	Al (wt.%)	Ti (wt.%)	Si (wt.%)	V (ppm)	Cr (ppm)	Mn (ppm)	Mo (ppm)	$\delta^{13}C_{org}$ (‰ vs. PDB)
114.25			8.59	0.40	28.10	151	51	333	0	− 28.04
115.44			8.32	0.41	28.70	158	79	284	0	− 29.55
116	0.24	1.25	8.15	0.38	26.5	164	90	264	0	
116.57	1.04	0.42	7.63	0.35	29.00	184	84	279	1	− 29.22
117.07	2.62	0.00	7.26	0.37	28.3	297	95	187	20	
117.77			8.22	0.37	27.50	178	84	216	5	− 28.89
118.31	2.26	0.00	7.8	0.38	26.3	175	103	193	2	
119			6.96	0.35	29.80	289	72	208	17	− 29.15
119.55	2.52	0.75	7.47	0.41	27.6	268	95	186	19	
120.2			7.34	0.35	28.80	180	73	187	13	− 28.92
120.78	3.66	5.58	7.11	0.32	26.00	149	92	263	5	
121.4			6.35	0.34	27.1	124	64	209	7	− 28.87
121.66	1.63	0.58	6.24	0.43	29.30	106	77	185	15	
122.08	0.58	2.92	7.38	0.43	28.70	129	90	274	0	
122.55			6.77	0.4	30.8	117	69	297	1	− 30.68
123.09	0.36	4.08	8.81	0.46	25.9	146	102	383	0	
123.68			8.37	0.4	28	136	86	325	0	− 29.99
124.8			7.72	0.38	26.1	133	73	382	0	− 30.12
125.96			7.45	0.41	27	119	72	311	0	− 29.49

Table A4
Data tabulation for Rhinestreet Formation study interval

Depth (m)	OC (wt.%)	$CaCO_3$ (wt.%)	N_{tot} (wt.%)	P_{tot} (wt.%)	$\delta^{34}S_{pyr}$ (‰ vs. CDT)
31.75	0.2	0.33			
31.8	0.72	0.33	0.06	0.040	
31.83	0.87	0.50			− 20.35
31.88	0.85	0.67	0.02		
31.98	0.5	0.75			
32.09	0.88	0.58			
32.12	0.87	0.58	0.04	0.040	
32.15	1.16	0.83			

(continued on next page)

Table A4 (*continued*)

Depth (m)	OC (wt.%)	$CaCO_3$ (wt.%)	N_{tot} (wt.%)	P_{tot} (wt.%)	$\delta^{34}S_{pyr}$ (‰ vs. CDT)
32.19	0.7	0.75			
32.27	1	1.25	0.06	0.040	
32.36	0.59	1.92			
32.4	0.98	0.67			
32.45	0.67	4.83	0.02	0.040	
32.52	1.05	0.67			
32.59	0.67	2.75	0.03		
32.67	1.81	1.25			
32.74	2.78	0.75			
32.84	3.54	0.83	0.06	0.040	
32.91	2.93	2.17			
33.09	1.99	2.42	0.05		
33.25	2.13	1.83			
33.43	2.29	0.50			
33.46	1.89	0.50	0.06	0.090	
33.54	1.02	0.92			
33.64	1.05	0.33	0.07		
33.67	1.18	0.42			
33.74	2.14	0.67			
33.82	1.59	0.58	0.04	0.090	
33.88	1.55	0.42			
33.99	1.15	0.50			
34.06	0.95	0.42	0.02		
34.25	0.93	9.00			
34.34	0.28	2.25	0.01	0.070	
34.5	0.69	0.58			
34.68	1.18	0.42	0.02		
34.75	2.07	0.33			
34.86	1.71	0.33	0.03	0.050	
34.93	2	0.33			
34.97	1.13	0.42	0.02		
35.05	1.17	0.67			
35.46	0.68	0.50			− 15.61
35.65	0.74	0.25	0.02	0.045	
35.85	1.74	0.33			
35.96	2.15	0.50	0.04		
36.18	2.83	0.58			
36.39	2.83	0.83			
36.59	3.07	1.83	0.09	0.040	− 24.33
36.8	2.73	2.00			
37.03	2.26	0.42			
37.25	1.32	0.67	0.05		
37.5	2	3.92			
37.73	1.43	0.75			
37.98	1.46	3.08	0.05	0.040	
38.22	1.21	2.75			
38.38	1.23	0.50	0.03		
38.68	1.89	4.42			
38.93	1.3	0.50	0.03	0.040	
39.04	1.91	0.33			
39.25	1.96	0.33			
39.39	1.76	0.33	0.05		
39.65	1.41	2.50			
39.9	1.7	0.58			

Table A4 (*continued*)

Depth (m)	OC (wt.%)	$CaCO_3$ (wt.%)	N_{tot} (wt.%)	P_{tot} (wt.%)	$\delta^{34}S_{pyr}$ (‰ vs. CDT)
39.98	1.8	0.50	0.04	0.040	
40.24	1.91	1.17			− 17.29
40.5	1.79	0.25			
40.6	1.66	0.50	0.05		
40.78	1.28	4.17			
41.14	1.01	1.92			
41.2	1.18	0.42	0.03	0.040	
41.35	1.29	1.17			
41.61	1.28	2.58			
41.81	2	0.33	0.04		
42.05	2	0.58	0.04	0.040	
42.26	1.56	2.00			
42.44	0.85	1.83	0.03		
42.65	1.37	1.92			
42.9	1.37	0.67	0.05	0.040	
43.1	1.38	1.50			
43.29	1.61	2.42			
43.5	1.4	0.58	0.05		
43.7	1.5	1.17			
43.9	1.56	0.75			
44.05	1.52	0.33	0.05	0.040	
44.25	1.18	2.17			
44.46	0.26	2.67			
44.66	0.33	3.50	0.03	0.040	− 10.42
44.86	0.48	1.25			
45.13	0.47	0.92			
45.35	0.47	2.83	0.04	0.040	
45.54	0.57	2.33			
45.74	1.14	1.00			
45.94	1.65	0.58	0.05		
46.15	2.45	0.67			− 16.84
46.35	2.04	0.58	0.05	0.040	
46.56	1.55	0.92			
46.77	0.78	5.25			
46.93	0.63	6.08	0.04		
47.13	0.59	5.17			
47.33	0.37	4.67			
47.74	0.41	1.92	0.03	0.040	
47.94	0.43	3.92			
48.35	0.45	1.83	0.04		
48.54	0.42	3.25			
48.73	0.62	2.50			− 8.37
48.94	0.66	2.42	0.04	0.040	
49.14	0.67	1.83			
49.34	0.52	2.25	0.04		
49.54	0.63	3.17			
49.74	0.83	2.42			
49.89	0.93	0.83	0.02	0.040	
50.11	1.83	1.33			
50.32	1.73	1.00	0.04		
50.52	1.73	1.42			
50.69	0.8	1.00	0.03	0.040	

(continued on next page)

Table A4 (*continued*)

Depth (m)	OC (wt.%)	$CaCO_3$ (wt.%)	N_{tot} (wt.%)	P_{tot} (wt.%)	$\delta^{34}S_{pyr}$ (‰ vs. CDT)
51.09	0.93	2.17			
51.27	1.25	2.42	0.04		
51.66	1.49	0.25			
51.84	1.72	0.42	0.05	0.037	
52.23	2.18	0.42			
52.42	2.3	0.50	0.06		
52.62	2.62	0.50			
52.82	3.14	0.50			
52.99	3.22	0.75	0.08	0.033	
53.38	3.4	0.50			
53.58	3.15	1.00			
53.78	3.26	1.08	0.07		− 10.40
53.97	2.36	0.58			
54.16	1.7	1.75			
54.37	1.98	1.50	0.06	0.030	
54.58	3.03	1.58			
54.98	2.64	3.25	0.08		
55.19	1.74	4.42			
55.6	0.63	7.08	0.04	0.040	
55.78	0.51	4.83			
55.98	0.43	7.25	0.03		
56.19	0.4	7.83			
56.37	0.36	5.83	0.04	0.050	
56.59	0.35	8.92	0.06		− 14.71
57.57	0.4733	6.00			
58.74	0.3495	5.12			

Depth (m)	Al (wt.%)	Ti (wt.%)	Si (wt.%)	V (ppm)	Cr (ppm)	Mn (ppm)	Mo (ppm)	$\delta^{13}C_{org}$ (‰ vs. PDB)
31.45	9.84	0.47	29.20	195	87	355	0	− 28.58
32.57	9.03	0.46	25.40	165	81	328	0	− 28.56
33.71	8.91	0.45	26.30	166	78	268	2	− 29.07
34.79	11.2	0.52	24.5	218	94	271	0	− 27.00
36.16	8.32	0.41	25.9	180	87	329	5	− 29.75
37.31	8.98	0.40	25.80	282	103	202	4	− 29.16
38.46	9.12	0.43	22.7	195	88	279	8	− 30.3
39.59	8.64	0.40	25.20	165	84	373	0	− 29.37
40.69	9.21	0.43	24.5	166	85	421	0	− 29.36
41.86	8.52	0.4	26.1	168	86	251	12	− 30.01
43	8.77	0.4	25.6	179	87	249	30	− 29.83
44.11	8.4	0.4	22.8	196	83	262	15	− 29.97
45.32	9.79	0.39	24.6	175	93	294	0	− 29.93
46.43	8.68	0.38	23.1	191	91	280	2	− 28.91
47.54	7.81	0.4	24.7	138	68	463	0	− 29.22
48.67	8.92	0.39	22.5	158	89	394	0	− 28.93
49.81	8.42	0.39	21.6	204	93	381	1	− 29.05
50.88	8.91	0.41	23.7	202	90	317	2	− 29.03
52.02	8.68	0.39	26	289	94	219	9	− 28.49
53.19	8	0.34	26.9	226	78	187	24	− 28.38
54.22	8.05	0.36	25	147	82	301	1	− 28.18
55.38	7.62	0.34	23.3	133	80	511	0	− 29.75
56.49	7.25	0.38	24.9	119	67	469	0	− 29.39
57.57	7.37	0.38	25.4	127	80	476	0	− 30.13
58.74	7.76	0.42	23.9	138	88	491	0	

Table A5
Data tabulation for Pipe Creek and Hanover formations study intervals

Depth (m)	OC (wt.%)	$CaCO_3$ (wt.%)	Al wt.%	Ti (wt.%)	Si (wt.%)	V (ppm)	Cr (ppm)	Mn (ppm)	Mo (ppm)	N_{tot} (wt.%)	P_{tot} (wt.%)	$\delta^{13}C_{org}$ (‰ vs. PDB)	$\delta^{13}S_{pyr}$ (‰ vs. CDT)
217.00	0.56	0.42	8.61	0.46	28.8	155	82	292	6			− 30.25	
222.99	2.24	0.33	6.15	0.31	30.9	110	62	235	37			− 28.94	
228.90	3.06	1.08	6.4	0.34	30.4	118	68	282	30			− 29.24	
230.98	2.63	0.08	5.8	0.32	31.3	110	61	186	36				
232.17	2.23	0.08	7.03	0.37	29.2	128	70	228	25			− 27.95	
233.30	0.61	0.58	8.79	0.42	27.3	147	81	268	0				
234.55	0.56	2.08	8.4	0.43	27.9	150	48	595	0				
235.16	0.27	2.25								0.029	0.0114	− 25.64	
235.20	0.31	3.67	8.22	0.36	27.3	138	69	456	0				
235.35	0.96	3.25	6.45	0.34		110	78	400	6	0.05		− 25.43	− 21.3
235.50	0.25	1.21	9.3	0.37	26.5	156	96	422	0				
235.55	1.22	16.50								0.107	0.0093	− 25.71	
235.70	0.58	1.83	9.59	0.41		161	110	1190	0	0.189		− 25.98	
235.80	0.26	9.54	6.39	0.35	26.3	106	53	709	0				
235.85	0.54	6.92								0.137		− 25.78	
236.00	0.22	10.75	7.44	0.41		115	93	715	0	0.048	0.0089	− 25.58	6.83
236.10	3.22	5.25	6.38	0.34	28.1	115	66	594	5				
236.15	0.21	12.33								0.028		− 26.33	
236.23	0.95	4.00								0.179		− 27.07	
236.35	2.55	7.50	6.12	0.34		103	80	644	3	0.204	0.0096	− 26.63	− 19.46
236.49	3.65	3.44	6.4	0.36	29.8	114	69	495	9				
236.51	2.62	7.83								0.143		− 26.19	
236.65	3.00	0.17	9.03	0.44		150	94	312	3	0.152	0.0124	− 26.69	
236.81	2.53	3.58								0.106		− 27.2	
236.84	2.63	0.15	7.17	0.38	29.5	128	74	306	13				
236.98	3.25	1.08	6.57	0.38		117	86	287	8	0.137	0.0084	− 27.42	− 19.15
237.00	2.94	0.42	6.71	0.33	30.9	119	70	307	18				
237.13	3.07	0.33								0.122		− 27.65	
237.24	2.56	0.00	6.99	0.37	30.1	126	73	284	29				
237.28	2.70	0.50								0.11	0.0078	− 27.79	
237.46	1.86	0.33	7.60	0.47		132	97	276	24	0.088		− 27.94	
237.64	0.13	5.49	5.58	0.34	33.1	88	36	421	0				
237.66	0.91	0.17								0.078	0.0087	− 27.43	
237.82	0.14	0.00	10.90	0.45		186	118	316	0	0.055		− 26.93	− 16.39
237.96	0.09	4.08								0.02	0.0112	− 27.53	
238.02	0.37	2.93	6.54	0.41	32	105	45	586	0				
238.11	0.06	7.00	5.55	0.39		83	63	598	0	0.043		− 28.12	
238.26	0.08	5.00								0.044	0.0122	− 28.39	
238.58	0.10	1.50	7.63	0.42		128	49	339	0	0.025		− 28.65	− 17
238.74	0.47	3.78	5.84	0.37	33	96	36	449	0				
239.14	1.86	0.00	5.45	0.38	29.6	113	62	255	16				
239.89	0.50	1.00	5.99	0.44	31.6	121	63	321	0			− 30.67	
240.96	0.63	0.33	6.08	0.41	29.9	122	67	254	0				
241.98	0.22	0.08	7.1	0.41	31.8	123	62	275	0				
243.34	0.43	1.33	7.82	0.4	28.6	140	73	254	2				
246.93	1.86	1.42	7.28	0.45	31.8	128	68	272	0			− 32.43	
273.06	0.30	6.33			27.5								
274.10	0.31	4.58								0.065	0.0048	− 27.12	
274.20	0.31	3.67								0.08		− 27.15	
274.30	0.28	3.58								0.038	0.0043	− 27.39	
274.45	0.49	2.08	8.30	0.39		146	92	218	0	0.042		− 27.17	

(continued on next page)

Table A5 (*continued*)

Depth (m)	OC (wt.%)	$CaCO_3$ (wt.%)	Al wt.%	Ti (wt.%)	Si (wt.%)	V (ppm)	Cr (ppm)	Mn (ppm)	Mo (ppm)	N_{tot} (wt.%)	P_{tot} (wt.%)	$\delta^{13}C_{org}$ (‰ vs. PDB)	$\delta^{13}S_{pyr}$ (‰ vs. CDT)
274.55	2.12	0.75								0.121	0.0335	− 27.6	
274.63	0.24	7.42								0.021		− 27.65	10.89
274.70	3.48	6.25								0.296		− 27.6	
274.75	0.86	2.58								0.103	0.0032	− 27.7	
274.79	3.69	6.83								0.217		− 26.97	
274.83	4.16	6.75	6.39	0.34		118	88	466	3	0.184		− 26.25	− 14.88
274.93	0.47	19.92			21.4								
275.17	3.94	5.17								0.178	0.0157	− 26.58	
275.32	3.41	4.42								0.16		− 26.87	
275.47	3.61	3.17	6.90	0.32		122	93	306	5	0.148	0.0155	− 27.49	
275.67	3.64	2.67								0.132		− 27.95	
275.83	4.29	3.17			29.7					0.142	0.0191	− 28.41	
275.98	3.35	2.00	6.81	0.31		121	94	312	2	0.121		− 28.63	
276.13	3.35	1.58								0.127	0.0112	− 28.85	
276.25	3.81	1.58								0.143		− 28.71	
276.40	4.41	2.17	6.23	0.3		109	86	309	1	0.163	0.0116	− 28.57	
276.43	4.75	1.51			27.7								
276.50	4.51	2.08								0.151		− 28.84	
276.65	3.97	2.08								0.125		− 28.72	
276.80	5.40	1.75	6.92	0.34		120	97	326	0	0.152	0.0155	− 29.11	− 13.71
276.95	3.64	1.50								0.132		− 29.09	
277.10	3.69	1.08			27.5					0.153		− 29.07	
277.25	3.96	0.92	7.26	0.36		125	98	277	2	0.159	0.0155	− 29.07	
277.40	4.43	1.17								0.17		− 28.84	
277.55	3.52	0.58								0.13	0.0137	− 28.62	
277.71	4.01	0.58	6.96	0.34		119	88	267	2	0.138		− 28.88	
277.85	2.71	1.00								0.103	0.0195	− 29.2	
278.01	0.44	3.42	3.99	0.27		55	54	391	0	0.021		− 29.13	− 0.61
278.16	1.69	0.25								0.083	0.0246	− 29.14	
278.31	2.29	0.42	8.04	0.41		136	99	309	0	0.096		− 29.3	
278.41	1.39	0.92								0.055		− 29.46	
278.51	1.62	0.75			25.7					0.065	0.0128	− 29.59	
278.61	2.05	0.25								0.089		− 29.53	
278.73	2.60	0.33	8.11	0.44		143	106	284	15	0.126		− 29.6	
278.83	2.51	0.25								0.143	0.0187	− 29.4	
278.98	0.90	0.75								0.071		− 29.4	
279.08	0.76	1.50								0.079	0.0224	− 29.21	
279.23	0.78	1.58	4.97	0.34		74	65	310	0	0.084		− 29.31	
279.33	0.83	1.42								0.095		− 29.36	
279.43	0.57	2.50								0.069	0.0220	− 29.41	
279.86	1.06	1.68			34.4								
280.23	0.49	0.33	10.40	0.51		191	121	360	0	0.061	0.0298	− 29.31	
280.32	0.57	1.33								0.074		− 29.53	
280.50	0.65	0.17								0.084		− 29.76	
280.60	0.69	0.33	9.49	0.49		171	110	350	0	0.094	0.0298	− 29.6	− 6.52

References

Algeo, T.J., Berner, R.A., Maynard, J.B., Scheckler, S.E., 1995. Late Devonian oceanic anoxic events and biotic crises: "rooted" in the evolution of vascular land plants? GSA Today 5, 64–66.

Aller, R.C., 1994. Bioturbation and remineralization of sedimentary organic matter: effects of redox oscillation. Chem. Geol. 114, 331–345.

Arthur, M.A., Sageman, B.B., 1994. Marine black shales: a review of depositional mechanisms and significance of ancient deposits. Annu. Rev. Earth Planet. Sci. 22, 499–551.

Arthur, M.A., Dean, W.E., Pratt, L.M., 1988. Geochemical and

climatic effects of increased marine organic carbon burial at the Cenomanian/Turonian boundary. Nature 335, 714–717.

Berner, R.A., 1980. Early diagenesis: a theoretical approach. In: Holland, H.D. (Ed.), Princeton Series in Geochemistry. Princeton Univ. Press, Princeton. 237 pp.

Berner, R.A., 1990. Atmospheric carbon dioxide levels over Phanerozoic time. Science 249, 1382–1386.

Berner, R.A., 1997. The rise of plants and their effect on weathering and atmospheric CO_2. Science 276, 544–546.

Berner, R.A., Canfield, D.E., 1989. A new model for atmospheric oxygen over Phanerozoic time. In: Miles, D.L. (Ed.), Water–Rock Interaction. WRI-6, Proceedings - International Symposium on Water–Rock Interaction, vol. 6, pp. 73–74.

Bertrand, P., Shimmield, G., Martinez, P., Grousset, F., Jorissen, F., Paterne, M., Pujol, C., Bouloubassi, I., Buat Menard, P., Peypouquet, J.P., Beaufort, L., Sicre, M.A., Lallier-Verges, E., Foster, J.M., Ternois, Y., 1996. The glacial ocean productivity hypothesis: the importance of regional temporal and spatial studies. Mar. Geol. 130, 1–9.

Betts, J.N., Holland, H.D., 1991. The oxygen content of the ocean bottom waters, the burial efficiency of organic carbon, and the regulation of atmospheric oxygen. Palaeogeogr. Palaeoclimatol. Palaeoecol. 97, 5–18.

Bidigare, R.R., Fluegge, A., Freeman, K.H., Hanson, K.L., Hayes, J.M., Hollander, D.J., Jasper, J.P., King, L.L., Laws, E.A., Milder, J., Millero, F.J., Pancost, R., Popp, B.N., Steinberg, P.A., Wakeham, S.G., 1997. Consistent fractionation of ^{13}C in nature and in the laboratory: growth-rate effects in some haptophyte algae. Glob. Biogeochem. Cycles 11 (2), 279–292.

Boyle, E.A., 1983. Chemical accumulation variation under the Peru current during the last 130,000 years. J. Geophys. Res. 88, 7667–7680.

Bralower, T.J., Thierstein, H.R., 1984. Organic carbon and metal accumulation rates in Holocene and mid-Cretaceous sediments: paleoceanographic significance. In: Brooks, J., Fleet, A.J. (Eds.), Marine Petroleum Source Rocks. Geological Society London Special Publication, vol. 26, pp. 345–369.

Brett, C.E., 1995. Sequence stratigraphy, biostratigraphy, and taphonomy in shallow marine environments. Palaios 10, 597–616.

Brett, C.E., Baird, G.C., 1986. Symmetrical and upward shallowing cycles in the Middle Devonian of New York State and their implications for the punctuated aggradational cycle hypothesis. In: Arthur, M.A., Garrison, R.E. (Eds.), Special Section: Milankovitch Cycles Through Geologic Time. Paleoceanography, vol. 1, pp. 431–445.

Brett, C.E., Baird, G.C., 1996. Middle Devonian sedimentary cycles and sequences in the northern Appalachian Basin. In: Witzke, B.J., Ludvigson, G.A., Day, J. (Eds.), Paleozoic Sequence Stratigraphy: Views from the North American Craton. Special Paper - Geological Society of America, vol. 306, pp. 213–241.

Brett, C.E., Baird, G.C., 1997. Epiboles, outages, and ecological evolutionary bioevents: taphonomy, ecological, and biogeographic factors. In: Brett, C.E., Baird, G.C. (Eds.), Paleontological Events, Stratigraphic, Ecological and Evolutionary Implications. Columbia Univ. Press, New York, pp. 249–284.

Brett, C.E., Baird, G.C., Miller, K.B., 1986. Sedimentary cycles and lateral facies gradients across a Middle Devonian shelf-to-basin ramp, Ludlowville Formation, Cayuga Basin. New York State Geological Association, 58th Annual Meeting: Field Trip Guidebook, pp. 81–127.

Brett, C.E., Dick, V.B., Baird, G.C., 1991. Comparative taphonomy and paleoecology of Middle Devonian dark gray and black shales facies from western New York. In: Landing, E., Brett, C.E. (Eds.), Dynamic Stratigraphy and Depositional Environments of the Hamilton Group (Middle Devonian) in New York State, Part II. New York State Museum Bulletin, vol. 469, pp. 5–36.

Buggisch, W., 1991. The global Frasnian–Famennian "Kellwasser Event". Geol. Rundsch. 80, 49–72.

Byers, C.W., 1977. Biofacies patterns in euxinic basins: a general model. In: Cook, H.E., Enos, P. (Eds.), Deep Water Carbonate Environments. Society of Economic Paleontologists and Mineralogists, Tulsa, pp. 5–17.

Calvert, S.E., Pedersen, T.F., 1996. Sedimentary geochemistry of manganese: implications for the environment of formation of manganiferous black shales. Econ. Geol. 91, 36–47.

Calvert, S.E., Bustin, R.M., Ingall, E.D., 1996. Influence of water column anoxia and sediment supply on the burial and preservation of organic carbon in marine shales. Geochim. Cosmochim. Acta 60, 1577–1593.

Canfield, D.E., 1994. Factors influencing organic carbon preservation in marine sediments. Chem. Geol. 114, 315–329.

Canfield, D.E., Lyons, T.W., Raiswell, R., 1996. A model for iron deposition to euxinic Black Sea sediments. Am. J. Sci. 296, 818–834.

Caplan, M.L., Bustin, R.M., 1996. Factors governing organic matter accumulation and preservation in a marine petroleum source rock from the Upper Devonian to Lower Carboniferous Exshaw Formation, Alberta. Bull. Can. Pet. Geol. 44, 474–494.

Caplan, M.L., Bustin, R.M., 1999. Devonian–Carboniferous Hangenberg mass extinction event, widespread organic-rich mudrock and anoxia: causes and consequences. Palaeogeogr. Palaeoclimatol. Palaeoecol. 148 (4), 187–207.

Copper, P., 1986. Frasnian–Famennian mass extinction and cold-water oceans. Geology 14, 835–839.

Crusius, J., Calvert, S., Pedersen, T., Sage, D., 1996. Rhenium and molybdenum enrichments in sediments as indicators of oxic, suboxic and sulfidic conditions of deposition. Earth Planet. Sci. Lett. 145, 65–78.

Dean, W.E., Piper, D.Z., Peterson, L.C., 1999. Molybdenum accumulation in Cariaco basin sediment over the past 24 k.y.: a record of water-column anoxia and climate. Geology 27, 507–510.

Demaison, G.J., Moore, G.T., 1980. Anoxic environments and oil source bed genesis. Am. Assoc. Pet. Geol. Bull. 64, 1179–1209.

DeNiro, M.J., Epstein, S., 1978. Influence of diet on the distribution of carbon isotopes in animals. Geochim. Cosmochim. Acta 42, 495–506.

Dennison, J.M., 1985. Catskill Delta shallow marine strata. In: Woodrow, D.L., Sevon, W.D. (Eds.), The Catskill Delta. Geological Society of America, Special Paper, vol. 201, pp. 91–106.

Durand, B. (Ed.), 1980. Kerogen: Insoluble Organic Matter from Sedimentary Rocks. Ed. Technip, Paris, p. 519.

Emerson, S., 1985. Organic carbon preservation in marine sediments. In: Sundquist, E.T., Broecker, W.S. (Eds.), The Carbon

Cycle and Atmospheric CO_2: Natural Variations Archean to Present. Geophysical Monograph, vol. 32, pp. 78–87.

Emerson, S., Hedges, J.I., 1988. Processes controlling the organic carbon content of open ocean sediments. Paleoceanography 3, 621–634.

Emerson, S.R., Huested, S.S., 1991. Ocean anoxia and the concentrations of molybdenum and vanadium in seawater. Mar. Chem. 34, 177–196.

Ettensohn, F.R., 1985a. The Catskill Delta complex and the Acadian Orogeny: a model. In: Woodrow, D.L., Sevon, W.D. (Eds.), The Catskill Delta. Geological Society of America, Special Paper, vol. 201, pp. 39–49.

Ettensohn, F.R., 1985b. Controls on development of Catskill Delta complex basin-facies. In: Woodrow, D.L., Sevon, W.D. (Eds.), The Catskill Delta. Geological Society of America, Special Paper, vol. 201, pp. 65–77.

Ettensohn, F.R., Barron, L.S., 1981. Depositional model for the Devonian–Mississippian black shales of North America: A paleoclimatic–paleogeographic approach. In: Roberts, T.J. (Ed.), GSA Field Trip Guidebook, Cincinnati, 1981. American Geological Institute, Falls Church, VA, pp. 344–361.

Ettensohn, F.R, Miller, M.L., Dillman, S.B., Elam, T.D., Geller, K.L., Swager, G., Markowitz, G.D., Woock, F.D., Barron, L.S., 1988. Characterization and implications of the Devonian–Mississippian black shale sequence, eastern and central Kentucky, U.S.A.: pycnoclines, transgression, and tectonism. In: McMillan, N.J., Embry, A.F., Glass, D.J. (Eds.), Devonian of the World, II. Canadian Society of Petroleum Geologists, Memoir, vol. 14, pp. 323–345.

Fillipelli, G., 1997. Controls on the phosphorus concentration and accumulation in marine sediments. Mar. Geol. 139, 231–240.

Fleming, R.H., Revelle, R., 1939. Physical Processes in the Ocean. In: Trask, P.D. (Ed.), Recent marine sediments. American Association Petroleum Geologists, Tulsa, OK, pp. 48–141.

Gong, C., Hollander, D.J., 1996. Differential contribution of bacteria to sedimentary organic matter in oxic and anoxic environments, Santa Monica Basin, California. Org. Geochem. 26, 545–563.

Grabau, A.W., 1913. Principles of Stratigraphy. Seiler, New York. 1185 pp.

Hamilton-Smith, T., 1993. Stratigraphic effects of the Acadian orogeny in the autochthonous Appalachian basin. In: Roy, D.C., Skehan, J.W. (Eds.), The Acadian Orogeny: Recent Studies in New England, Maritime Canada, and the Autochthonous Foreland. Geological Society of America, Special Paper, vol. 275, pp. 153–164. Boulder, CO.

Hartnett, H.E., Keil, R.G., Hedges, J.I., Devol, A.H., 1998. Influence of oxygen exposure time on organic carbon preservation in continental margin sediments. Nature 391, 572–574.

Hayes, J.M., Takigiku, R., Ocampo, R., Callot, H., Albrecht, P., 1987. Isotopic compositions and probable origins of organic molecules in the Eocene Messel Shale. Nature 329, 48–51.

Hayes, J.M., Freeman, K.F., Popp, B.N., Hoham, C.H., 1990. Compound specific isotopic analysis: a novel tool for reconstruction of ancient biogeochemical processes. Org. Geochem. 16, 1115–1128.

Heckel, P.H., Witzke, B.J., 1979. Devonian world paleogeography determined from distribution of carbonates and related lithic paleoclimatic indicators. Paleontological Association, Special Paper, vol. 23, pp. 99–123.

Helz, G.R., Miller, C.V., Charnock, J.M., Mosselmans, J.F.W., Patrick, R.A.D., Garner, C.D., Vaughan, D.J., 1996. Mechanism of molybdenum removal from the sea and its concentration in black shales: EXAFS evidence. Geochim. Cosmochim. Acta 60, 3631–3642.

Henrichs, S.M., Reeburgh, W.S., 1987. Anaerobic mineralization of marine sediment organic matter: rates and the role of anaerobic processes in the oceanic carbon economy. Geomicrobiol. J. 5, 191–238.

House, M.R., 1981. Lower and Middle Devonian goniatite biostratigraphy. In: Oliver Jr., W.A., Klapper, G. (Eds.), Devonian Biostratigraphy of New York, Part 1. International Union of Geological Sciences, Subcommission on Devonian Stratigraphy, Washington, DC, pp. 33–37.

House, M.R., Kirchgasser, W.T., 1993. Devonian goniatite biostratigraphy and timing of facies movements in the Frasnian of eastern North America. In: Hailwood, E.A., Kidd, R.B. (Eds.), High Resolution Stratigraphy. Geological Society Special Publication, vol. 70, pp. 267–292.

Ibach, L.E.J., 1982. Relationship between sedimentation rate and total organic carbon content in ancient marine sediments. Am. Assoc. Pet. Geol. Bull. 66, 170–188.

Ingall, E., Jahnke, R., 1997. Influence of water-column anoxia on the elemental fractionation of carbon and phosphorus during sediment diagenesis. Mar. Geol. 139, 219–229.

Ingall, E.D., Bustin, R.M., Van Cappellen, P., 1993. Influence of water column anoxia on the burial and preservation of carbon and phosphorus in marine shales. Geochim. Cosmochim. Acta 57, 303–316.

Isaacson, P.E., Grader, G.W., Diaz-Martinez, E., 1997. Late Devonian glaciation (Famennian) in Gondwana and forced marine regression in North America, Geological Society of America, 1997 Annual Meeting. Abstr. Programs - Geol. Soc. Am. 29 (6), 117.

Joachimski, M.M., 1997. Comparison of organic and inorganic carbon isotope patterns across the Frasnian–Famennian boundary. Palaeogeogr. Palaeoclimatol. Palaeoecol. 132, 133–145.

Joachimski, M.M., Ostertag-Henning, C., Pancost, R.D., Strauss, H., Freeman, K.H., Littke, R., Sinninghe Damste, J.S., Racki, G., 2001. Water column anoxia, enhanced productivity and concomitant changes in $\delta^{13}C$ and $\delta^{34}S$ across the Frasnian–Famennian boundary (Kowala–Holy Cross Mountains/Poland). Chem. Geol. 175, 109–131.

Johnson, J.G., Sandberg, C.A., 1988. Devonian eustatic events in the western United States and their biostratigraphic responses. In: McMillan, N.J., Embry, A.F., Glass, D.J. (Eds.), Devonian of the World, III: Calgary, Alberta. Canadian Society of Petroleum Geologists, Memoir, vol. 14, pp. 171–178.

Kauffman, E.G., 1981. Ecological reappraisal of the German Posidonienschiefer (Toarcian) and the stagnant basin model. In: Gray, J., Boucot, A.J., Berry, W.B.N. (Eds.), Communities of the Past. Hutchinson Ross Publ., Stroudsburg, pp. 311–381.

Kepferle, R.C., 1993. A depositional model and basin analysis for the gas-bearing black shale (Devonian and Mississippian) in the Appalachian Basin. In: Roen, J.B., Kepferle, R.C. (Eds.), Petroleum Geology of the Devonian and Mississippian Black Shale

of Eastern North America. U.S. Geological Survey Bulletin, vol. 1909, pp. F1–F23.

Kirchgasser, W.T., Over, D.J., Woodrow, D.L., 1994. Frasnian (Upper Devonian) strata of the Genesee River Valley, western New York state. In: Brett, C.E., Scatterday, J. (Eds.), New York State Geological Association, 66th Annual Meeting Field Trip Guidebook, pp. 325–358.

Klapper, G., 1971. Sequence within the conodont genus *Polygnathus* in the New York lower Middle Devonian. Geol. Palaeontol. 5, 59–79.

Klapper, G., 1981. Review of New York Devonian conodont biostratigraphy. In: Oliver Jr., W.A., Klapper, G. (Eds.), Devonian Biostratigraphy of New York, Part 1. International Union of Geological Sciences, Subcommission on Devonian Stratigraphy, Washington, DC, pp. 57–66.

Klapper, G., Becker, R.T., 1999. Comparison of Frasnian (Upper Devonian) conodont zonations. Boll. Soc. Paleontol. Ital. 37, 339–348.

Kump, L.R., Arthur, M.A., 1999. Interpreting carbon-isotope excursions: carbonates and organic matter. Chem. Geol. 161, 181–198.

Kuypers, M.M.M., Blokker, P., Hopmans, E.C., Kinkel, H., Pancost, R.D., Schouten, S., Sinninghe Damste, J., 2002. Archeal remains dominate marine organic matter from the early Albian ocean anoxic event Ib. Palaeogeography, Palaeoclimatology, Palaeoecology 185, 211–234.

Lyons, T.W., 1997. Sulfur isotopic trends and pathways of iron sulfide formation in upper Holocene sediments of the anoxic Black Sea. Geochim. Cosmochim. Acta 61, 3367–3382.

Lyons, T.W., Werne, J.P., Hollander, D.J., 2002. Contrasting sulfur geochemistry and Fe/Al and Mo/Al ratios across the last oxic-to-anoxic transition in the Cariaco Basin, Venezuela. Chem. Geol. 195, 131–157 (this volume).

Martin, R.E., 1996. Secular increase in nutrient levels through the Phanerozoic: implications for productivity, biomass, and diversity of the marine biosphere. Palaios 11, 209–219.

McCollum, L.B., 1988. A shallow epeiric sea interpretation for an offshore Middle Devonian black shale facies in eastern North America. In: McMillan, N.J., Embry, A.F., Glass, D.J. (Eds.), Devonian of the World II. Canadian Society of Petroleum Geologists, Memoir, vol. 14, pp. 347–355.

McGhee Jr., G.R., 1996. The Late Devonian Mass Extinction: The Frasnian/Famennian Crisis. Columbia Univ. Press, New York. 303 pp.

McGhee, G.R., Sutton, R.G., 1985. Late Devonian marine ecosystems of the lower West Falls Group in New York. In: Woodrow, D.L., Sevon, W.D. (Eds.), The Catskill Delta. Geological Society of America, Special Paper, vol. 201, pp. 199–210.

McManus, J., Berelson, W.M., Coale, K.H., Johnson, K.S., Kilgore, T.E., 1997. Phosphorus regeneration in continental margin sediments. Geochim. Cosmochim. Acta 61, 2891–2907.

Meyers, P.A., 1994. Preservation of elemental and isotopic source identification of sedimentary organic matter. Chem. Geol. 114, 289–302.

Middelburg, J.J., Calvert, S.E., Karlin, R., 1991. Organic-rich transitional facies in silled basins: response to sea-level change. Geology 19, 679–682.

Murphy, A.E., 2000. Physical and biogeochemical mechanisms of black shale deposition, and their implications for ecological and evolutionary change in the Devonian Appalachian basin. Unpublished PhD dissertation, Northwestern University, 363 pp.

Murphy, A.E., Sageman, B.B., Hollander, D.J., 1998. Interpreting sea-level change from carbon isotopic shifts in organic matter: examples from the Devonian Appalachian Basin. Abstr. Programs-Geol. Soc. Am. 30, 396.

Murphy, A.E., Sageman, B.B., Hollander, D.J., Ver Straeten, C.A., 2000a. Organic carbon burial and faunal dynamics in the Appalachian basin during the Devonian (Givetian–Famennian) greenhouse: an integrated paleoecological/biogeochemical approach. In: Huber, B., MacLeod, K., Wing, S. (Eds.), Warm Climates in Earth History. Cambridge Univ. Press, Cambridge, UK, pp. 351–385.

Murphy, A.E., Sageman, B.B., Hollander, D.J., Lyons, T.W., Brett, C.E., 2000b. Black shale deposition in the Devonian Appalachian Basin: siliciclastic starvation, episodic water-column mixing, and efficient recycling of biolimiting nutrients. Paleoceanography 15, 280–291.

Murphy, A.E., Sageman, B.B., Hollander, D.J., 2000c. Eutrophication by decoupling of the marine biogeochemical cycles of C, N, and P: a mechanism for the Late Devonian mass extinction. Geology 28, 427–430.

Nijenhuis, I.A., Becker, J., DeLange, G.J., 2001. Geochemistry of coeval sediments in Mediterranean ODP cores and a land section: implications for sapropel formation models. Palaeogeogr. Palaeoclimatol. Palaeoecol. 165, 97–112.

Oschmann, W., 1991. Anaerobic–poikiloaerobic–aerobic: a new facies zonation for modern and ancient neritic redox facies. In: Einsele, G., Ricken, W., Seilacher, A. (Eds.), Cycles and Events in Stratigraphy. Springer-Verlag, Berlin, pp. 565–571.

Over, D.J., 1997. Conodont biostratigraphy of the Java Formation (Upper Devonian) and the Frasnian–Famennian boundary in western New York State. In: Klapper, G., Murphy, M.A, Talent, J.A. (Eds.), Paleozoic Sequence Stratigraphy, Biostratigraphy and Biogeography: Studies in Honor of J. Granville ("Jess") Johnson. Geological Society of America, Special Paper, vol. 321, pp. 161–177.

Pashin, J.C., Ettensohn, F.R., 1991. Paleoecology and sedimentology of the dysaerobic Bedford fauna (Late Devonian), Ohio and Kentucky (USA). Palaeogeogr. Palaeoclimatol. Palaeoecol. 91, 470–483.

Pedersen, T.F., Calvert, S.E., 1990. Anoxia vs. productivity: what controls the formation of organic-carbon-rich sediments and sedimentary rocks? Am. Assoc. Pet. Geol. Bull. 74, 454–466.

Pepper, J.F., de Witt Jr., W., 1951. The stratigraphy of the Perrysburg Formation of Late Devonian age in western and west-central New York. U.S. Geological Society Oil and Gas Investigations Chart OC-45, 2 sheets.

Piper, D.Z., 1994. Seawater as the source of minor elements in black shales, phosphorites and other sedimentary rocks. Chem. Geol. 114, 95–114.

Pompeckj, J.F., 1901. Die Juraablagerungen zwischen Regensburg und Regenstauf. Geogr. Jahrb. 14, 139–220.

Popp, B.N., Laws, E.A., Bidigare, R.R., Dore, J.E., Hanson, K.L., Wakeham, S.G., 1998. Effect of phytoplankton cell geometry on

carbon isotopic fractionation. Geochim. Cosmochim. Acta 62, 69–77.
Potter, P.E., Maynard, J.B., Pryor, W.A., 1982. Appalachian gas bearing shales: statement and discussion. Oil Gas J. 80, 290–318.
Pratt, L.M., 1984. Influence of paleoenvironmental factors on preservation of organic matter in the Middle Cretaceous Greenhorn Formation, Pueblo, CO. Am. Assoc. Pet. Geol. Bull. 68, 1146–1159.
Prave, A.R., Duke, W.L., Slattery, W., 1996. A depositional model for storm- and tide-influenced prograding siliciclastic shorelines from the Middle Devonian of the central Appalachian foreland basin USA. Sedimentology 43, 611–629.
Raiswell, R., Canfield, D.C., 1998. Sources of iron for pyrite formation in marine sediments. Am. J. Sci. 298, 219–245.
Raiswell, R., Buckley, F., Berner, R.A., Anderson, T.F., 1988. Degree of pyritization of iron as a paleoenvironmental indicator of bottom water oxygenation. J. Sediment. Petrol. 58, 812–819.
Redfield, A.C., Ketchum, B.H., Richards, F.A., 1963. The influence of organisms on the composition or seawater. In: Hill, M.N. (Ed.), The Sea, vol. 2. Wiley-Interscience, New York, pp. 26–77.
Retallack, G.J., 1997. Early forest soils and their role in Devonian global change. Science 276, 583–585.
Rickard, L.V., 1975. Correlation of the Devonian rocks in New York State. New York Museum and Science Service, Map and Chart Series, No. 24.
Rohl, H.-J., Schmid-Rohl, A., Oschmann, W., Frimmel, A., Schwark, L., 2001. The Posidonia shale (Lower Toarcian) of SW Germany: an oxygen-depleted ecosystem controlled by sea-level and palaeoclimate. Palaeogeogr. Palaeoclimatol. Palaeoecol. 165, 27–52.
Sageman, B.B., 1985. High-resolution stratigraphy and paleobiology of the Hartland Shale Member: analysis of an oxygen-deficient epicontinental sea. In: Pratt, L.M., Kaufmann, E.G., Zelt, F.B. (Eds.), Fine-Grained Deposits and Biofacies of the Cretaceous Western Interior Seaway: Evidence of Cyclic Sedimentary Processes. Society Economic Paleontologists and Mineralogists Field Trip Guidebook, vol. 4, pp. 110–121.
Sageman, B.B., Wignall, P.B., Kauffman, E.G., 1991. Biofacies models for organic-rich facies: tool for paleoenvironmental analysis. In: Einsele, G., Seilacher, A., Ricken, W. (Eds.), Cycles and Events in Stratigraphy. Springer Verlag, Berlin, pp. 542–564.
Saelen, G., Tyson, R.V., Talbot, M.R., Telnaes, N., 1998. Evidence of recycling of isotopically light CO_2(aq) in stratified black shale basins: contrasts between the Whitby Mudstone and Kimmeridge Clay formations, United Kingdom. Geology 26, 747–750.
Sarnthein, M., Pflaumann, U., Ross, R., Tiedemann, R., Winn, K., 1992. Transfer functions to reconstruct ocean palaeoproductivity: a comparison. In: Summerhayes, C.P., Prell, W.L, Emeis, K.-C. (Eds.), Upwelling Systems: Evolution Since the Early Miocene. Geological Society London Special Publication, vol. 64, pp. 411–427.
Schieber, J., 1999. Distribution and deposition of mudstone facies in the Upper Devonian Sonyea Group of New York. J. Sediment. Res. 69, 909–925.
Schieber, J., Krinsley, D., Riciputi, L., 2000. Diagenetic origin of quartz silt in mudstones and implications for silica cycling. Nature 406, 981–985.
Scholle, P.A., Arthur, M.A., 1980. Carbon isotope fluctuations in Cretaceous pelagic limestones: potential stratigraphic and petroleum exploration tool. Am. Assoc. Pet. Geol. Bull. 64, 67–87.
Scotese, C.R., McKerrow, W.S., 1990. Revised world maps and introduction. In: McKerrow, W.S., Scotese, C.R. (Eds.), Paleozoic Paleogeography and Biogeography. Geological Society, Memoir, vol. 12, pp. 1–21.
Scotese, C.R., Barrett, S.F., Van der Voo, R., 1985. Silurian and Devonian base maps. Philos. Trans. R. Soc. Lond., B 309, 57–77.
Schuchert, C., 1915. The conditions of black shale deposition as illustrated by Kuperschiefer and Lias of Germany. Proc. Am. Philos. Soc. 54, 259–269.
Schimmield, G.B., 1992. Can sediment geochemistry record changes in costal upwelling palaeoproductivity? Evidence from Northwest Africa and the Arabian Sea. In: Summerhayes, C.P., Prell, W.L., Emeis, K.-C. (Eds.), Upwelling systems: evolution since the early Miocene. Geological Society Special Publication, vol. 28, pp. 29–46.
Stach, E., Mackowsky, M.T., Teichmueller, M., Taylor, G.H., Chandra, D., Teichmueller, R., 1982. Stach's Textbook of Coal Petrology. Schweizerbart'sche Verlagbuchhandlung, Stuttgart. 569 pp.
Stein, R., 1986. Surface-water paleo-productivity as inferred from sediments deposited in oxic and anoxic deep-water environments of the Mesozoic Atlantic Ocean. In: Degens, E.T., Meyers, P.A., Brasell, S.C. (Eds.), Biogeochemistry of Black Shales: Case Studies From a Workshop. Mitteilungen aus dem Geologisch-Palaeontologischen Institut der Universitaet Hamburg, vol. 60, pp. 55–70.
Stein, R., 1990. Organic carbon/sedimentation rate relationship and its paleoenvironmental significance for marine sediments. Geo-Mar. Lett. 10, 851–867.
Stumm, W., Morgan, J.J., 1981. Aquatic Chemistry: An Introduction Emphasizing Chemical Equilibria in Natural Waters. Wiley, New York, p. 780.
Suess, E., 1980. Particulate organic carbon flux in the oceans: surface productivity and oxygen utilization. Nature 288, 260–263.
Thompson, J.B., Newton, C.R., 1987. Ecological reinterpretation of the dysaerobic Leiorhyncus fauna, Upper Devonian Geneseo black shale, central New York. Palaios 2, 274–281.
Tucker, R.D., Bradley, D.C., Ver Straeten, C.A., Harris, A.G., Ebert, J., McCutcheon, S.R., 1998. New U–Pb zircon ages and the duration and division of Devonian time. Earth Planet. Sci. Lett. 158, 175–186.
Twenhofel, W.H., 1915. Notes on black shale in the making. Am. J. Sci. 40, 272–280.
Tyrrell, T., Law, C.S., 1997. Low nitrate-phosphate ratios in the global ocean. Nature 387, 793–796.
Tyson, R.V., 1995. Sedimentary Organic Matter: Organic Facies and Palynofacies. Chapman & Hall, London. 615 pp.
Tyson, R.V., 2001. Sedimentation rate, dilution, preservation and total organic carbon: some results of a modeling study. Org. Geochem. 32, 333–339.
Tyson, R.V., Pearson, T.H., 1991. Modern and ancient continental

shelf anoxia: an overview. In: Tyson, R.V., Pearson, T.H. (Eds.), Modern and Ancient Continental Shelf Anoxia. Geological Society Special Publication, vol. 58, pp. 1–24.

Van Cappellen, P., Ingall, E.D., 1994. Benthic phosphorus regeneration, net primary production, and ocean anoxia: a model of the coupled marine biogeochemical cycles of carbon and phosphorus. Paleoceanography 9, 677–692.

Van der Voo, R., 1983. Paleomagnetic constraints on the assembly of the Old Red Continent. Tectonophysics 91, 271–283.

Van Der Zwann, G.J., Jorissen, F.J., 1991. Biofacial patterns in River induced shelf anoxia. In: Tyson, R.V., Pearson, T.H. (Eds.), Modern and Ancient Continental Shelf Anoxia. Geological Society Special Publication, vol. 58, pp. 65–82.

Ver Straeten, C.A., Brett, C.E., 1995. Lower and Middle Devonian foreland basin fill in the Catskill Front: stratigraphic synthesis, sequence stratigraphy, and the Acadian Orogeny. In: Garver, J.I., Smith, J.A. (Eds.), New York State Geological Association, 67th Annual Meeting Field Trip Guidebook, pp. 313–356.

Ver Straeten, C.A., Griffing, D.H., Brett, C.E., 1994. The lower part of the Middle Devonian Marcellus "Shale", central to western New York State: stratigraphy and depositional history. In: Brett, C.E., Scatterday, J. (Eds.), New York State Geological Association, 66th Annual Meeting Field Trip Guidebook, pp. 271–321.

Werne, J.P., Hollander, D.J., Lyons, T.W., Peterson, L.C., 2000. Climate-induced variations in productivity and planktonic ecosystem structure from the Younger Dryas to Holocene in the Cariaco Basin, Venezuela. Paleoceanography 15, 19–29.

Werne, J.P., Sageman, B.B., Lyons, T.W., Hollander, D.J., 2002. An integrated assessment of a "type euxinic" deposit: evidence for multiple controls on black shale deposition in the middle Devonian Oatka Creek Formation. Am. J. Sci. 302, 110–143.

Wignall, P.B., 1994. Black Shales. Clarendon Press, Oxford. 127 pp.

Wignall, P.B., Hallam, A., 1991. Biofacies, stratigraphic distribution, and depositional models of British onshore Jurassic black shales. In: Tyson, R.V., Pearson, T.H. (Eds.), Modern and Ancient Continental Shelf Anoxia. Geological Society Special Publication, vol. 58, pp. 291–309.

Witzke, B.J., Heckel, P.H., 1988. Paleoclimatic indicators and inferred Devonian paleolatitudes of Euramerica. In: McMillan, N.J., Embry, A.F., Glass, D.J. (Eds.), Devonian of the World, I. Canadian Society of Petroleum Geologists, Memoir, vol. 14, pp. 49–63.

Woodrow, D.L., 1985. Paleogeography, paleoclimate, and sedimentary processes of the Late Devonian Catskill Delta. In: Woodrow, D.L., Sevon, W.D. (Eds.), The Catskill Delta. Geological Society of America, Special Paper, vol. 201, pp. 51–63.

Woodrow, D.L., Fletcher, F.W., Ahrnsbrak, W.F., 1973. Paleogeography and paleoclimate at the depositional sites of the Devonian Catskill and Old Red Facies. Geol. Soc. Amer. Bull. 84, 3051–3064.

Woodrow, D.L., Dennison, J.M., Ettensohn, F.R., Sevon, W.T., Kirchgasser, W.T., 1988. Middle and Upper Devonian stratigraphy and paleogeography of the central and southern Appalachians and eastern Midcontinent, U.S.A. In: McMillan, N.J., Embry, A.F., Glass, D.J. (Eds.), Devonian of the World, I. Canadian Society of Petroleum Geologists, Memoir, vol. 14, pp. 277–301.

Wortmann, U.G., Hesse, R., Zacher, W., 1999. Major element analysis of cyclic black shales: paleoceanographic implications for the Early Cretaceous deep western Tethys. Paleoceanography 14, 525–541.

Yochelson, E.L., Lindemann, R.H., 1986. Considerations on the systematic placement of the Styliolines (incertae sedis: Devonian). In: Hoffman, A., Nitecki, N.H. (Eds.), Problematic Fossil Taxa. Oxford Monographs in Geology and Geophysics, vol. 5, pp. 45–58.